Geobiology (2006), **4**, 239–269 DOI: 10.1111/j.1472-4669.2006.00084.x

Biogeochemical modelling of the rise in atmospheric oxygen

M. W. CLAIRE,[1] D. C. CATLING[2,3] AND K. J. ZAHNLE[4]

[1]*Department of Astronomy, University of Washington, Box 351580, Seattle, WA 98195, USA*
[2]*Department of Earth Sciences, University of Bristol, Wills Memorial Building, Queen's Road, Bristol BS8 1RJ, UK*
[3]*Department of Atmospheric Sciences, University of Washington, Box 351640, Seattle, WA 98195, USA*
[4]*Mail Stop 245-3, Space Science Division, NASA Ames Research Center, Moffett Field, CA 94035, USA*

ABSTRACT

Understanding the evolution of atmospheric molecular oxygen levels is a fundamental unsolved problem in Earth's history. We develop a quantitative biogeochemical model that simulates the Palaeoproterozoic transition of the Earth's atmosphere from a weakly reducing state to an O_2-rich state. The purpose is to gain an insight into factors that plausibly control the timing and rapidity of the oxic transition. The model uses a simplified atmospheric chemistry (parameterized from complex photochemical models) and evolving redox fluxes in the Earth system. We consider time-dependent fluxes that include organic carbon burial and associated oxygen production, reducing gases from metamorphic and volcanic sources, oxidative weathering, and the escape of hydrogen to space. We find that the oxic transition occurs in a geologically short time when the O_2-consuming flux of reducing gases falls below the flux of organic carbon burial that produces O_2. A short timescale for the oxic transition is enhanced by a positive feedback due to decreasing destruction of O_2 as stratospheric ozone forms, which is captured in our atmospheric chemistry parameterization. We show that one numerically self-consistent solution for the rise of O_2 involves a decline in flux of reducing gases driven by irreversible secular oxidation of the crust caused by time-integrated hydrogen escape to space in the preoxic atmosphere, and that this is compatible with constraints from the geological record. In this model, the timing of the oxic transition is strongly affected by buffers of reduced materials, particularly iron, in the continental crust. An alternative version of the model, where greater fluxes of reduced hydrothermal cations from the Archean seafloor consume O_2, produces a similar history of O_2 and CH_4. When climate and biosphere feedbacks are included in our model of the oxic transition, we find that multiple 'Snowball Earth' events are simulated under certain circumstances, as methane collapses and rises repeatedly before reaching a new steady-state.

Received 15 March 2006; accepted 31 July 2006

Corresponding author: M. W. Claire, Tel.: 206-616-4549; fax: 206 685-0403: e-mail: mclaire@astro.washington.edu.

1. INTRODUCTION

Oxygen is the third most abundant element in the cosmos (Anders & Grevesse, 1989) and the most abundant element in the composition of the Earth (Kargel & Lewis, 1993). Most of Earth's oxygen atoms are bound up in rocks (silicates and iron oxides) and water, with only a small portion (<1 in 10^6) existing in molecular gaseous form (i.e., O_2, 'free' or 'atmospheric' oxygen). Modern levels of atmospheric oxygen sustain virtually all multicellular life (Catling *et al.*, 2005), and recent geochemical work has confirmed the long-held hypothesis that oxygen levels have not remained constant over geological time. Recent summaries of the geological evidence are provided by Canfield (2005), Catling & Claire (2005) and Holland (2006), and are summarized in Fig. 1. Taken as a whole, the data separate two periods of Earth's history. Prior to ~2.4 Ga (billion years ago), atmospheric oxygen did not leave the characteristic signatures of oxidation that are prevalent in the geological record from 2.4 Ga to the present. This paper presents a quantitative examination of processes related to the timing and nature of this transition, named the 'Great Oxygenation Event' (GOE) by Holland (2002).

2. THEORIES FOR THE RISE IN OXYGEN

2.1 Sources vs. sinks of O_2

In the modern atmosphere, free oxygen is relentlessly destroyed by reactions with reduced gases emanating from volcanoes and hot springs, and by the oxidation of the continents (i.e.

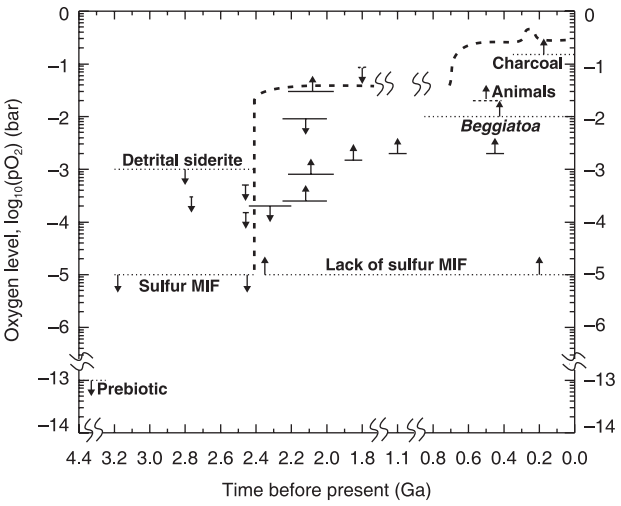

Fig. 1 A compilation of upper and lower bounds on oxygen concentration from the literature, updated from the version in Catling & Claire (2005). A possible evolutionary path for atmospheric oxygen is sketched as a thick dashed line. Palaeosols are shown as thick lines, with the width of the line corresponding to the age uncertainty (Rye & Holland, 1998). Updated constraints from the Hekpoort palaeosol are shown (Yang & Holland, 2003), although others interpret a higher lower limit on pO_2 from this soil (Beukes *et al*., 2002). Constraints shown as dotted lines pertain to the entire time span of their width. Dotted line constraints are taken from the presence and absence of mass-independent fractionation in sulfur isotopes (MIF) (Pavlov & Kasting, 2002), although see Zahnle *et al*. (2006) for an additional viewpoint; presence of detrital siderite (Rasmussen & Buick, 1999); sulfidic deep waters at 1.84 Ga (Poulton *et al*., 2004; Canfield, 2005); and the O_2 requirements of *Beggiatoa* (Canfield & Teske, 1996); animals (Runnegar, 1991); charcoal production (Chaloner, 1989). Phanerozoic oxygen curve is abstracted from models based on carbon and sulfur isotope data (Berner *et al*., 2003).

kerogen oxidation and the 'rusting' of exposed iron rich rocks). Holland (2002) estimates this modern rate of free oxygen destruction at 17.9 ± 8.5 Tmol year^{-1}. Left unbalanced, destruction rates of this magnitude would deplete the atmospheric reservoir of free oxygen (3.4×10^7 Tmol O_2 (Petsch, 2004)) on the order of millions of years, implying that there must be a continuous source to balance these geological sinks.

The source is chiefly biological. Virtually all atmospheric oxygen derives from a single metabolism, oxygenic photosynthesis. The net redox reaction that this metabolism exploits can be loosely described by the following equation, where 'CH_2O' approximates the average stoichiometry of organic matter:

$$CO_2 + H_2O \rightarrow CH_2O + O_2 \qquad (1)$$

To first order, respiration and decay (the reverse of equation 1) rapidly consume all of the free oxygen liberated, so oxygenic photosynthesis by itself does not constitute a net source of free oxygen. It is only when the organic carbon produced by a photosynthesizer escapes re-oxidation by burial in sediments, that oxygen is effectively added to the system. The modern net free oxygen source of 10 Tmol year^{-1} is supported by the burial of ~10 Tmol year^{-1} of photosynthetically derived organic carbon in sediments on the continental shelves (Holland, 1978; pp. 215–219). By contrast, land-based photosynthesis provides a negligible net oxygen source despite its large gross flux, given the lesser area available for permanent burial of organic carbon (Field *et al*., 1998). In addition, land-based plants did not evolve until the Phanerozoic (Kenrick & Crane, 1997), and so are not relevant to discussions regarding Archean and Proterozoic oxygen levels.

The other major source of oxidizing power to the Earth system is the escape of hydrogen atoms or molecules from the top of the atmosphere. This process ultimately oxidizes the reservoir from which the hydrogen originated. The reason for oxidation is that hydrogen was primarily delivered to Earth as H_2O, hydrated silicates, and hydrocarbons, given that any H_2 captured directly from the solar nebula would have been lost by subsequent impact erosion (Ahrens, 1993). Hydrogen that escapes ultimately originates by splitting hydrogen from one of these compounds, leaving behind an oxidized product to balance the redox reaction. Regardless of how the hydrogen atom is transported to the upper atmosphere (i.e. as CH_4, H_2O, H_2, or some other H-bearing compound), escape of that hydrogen atom implies that the reservoir from which it originated has been oxidized to balance the reduction of hydrogen from its bound form (an oxidation number of +1) to the elemental form (an oxidation number of 0). In the modern day, hydrogen escape is limited by the abundance of H-bearing compounds in the lower stratosphere (Walker, 1977; pp. 157–163) that contains ~1.7 ppmv of CH_4, 0.5 ppmv of H_2, and 3 ppmv of H_2O (Harries *et al*., 1996). Unlike H_2O, CH_4 does not condense in the troposphere, and hence can act as a quantitatively significant carrier of hydrogen to the upper atmosphere. Given the antiquity of the methanogenic metabolism (Hayes, 1994; Brocks *et al*., 1999, 2003) and arguments for enhanced levels of Archean CH_4 (Pavlov *et al*., 2000), oxidation due to escape of H associated with CH_4 may have played an important role during the Archean (Catling *et al*., 2001).

The only significant abiotic source of free oxygen is the photodissociation of H_2O with subsequent loss of hydrogen atoms to space (with a net reaction, $2H_2O + h\nu \rightarrow O_2 + 4H\uparrow$). Without the escape of hydrogen, the photodissociation products are free to recombine. Similarly, photodissociation of CO_2 is not a net source of free O_2, unless photochemically coupled to hydrogen escape, given that the photochemical products recombine quickly. A cold stratosphere forces water vapor to condense in the upper (tropical) troposphere, trapping water below the level where there are sufficient UV photons available for photolysis. This condensable nature of H_2O limits the supply of hydrogen to space and renders this source of abiotic O_2 insignificant. Although the modern tropopause temperature minimum is connected to the presence of the ozone layer, condensation of clouds and a temperature minimum are common features of planetary atmospheres, so that we expect cold-trapping of water vapor to be limiting on early

Earth. Well-defined tropopauses are found on Neptune, Saturn, Titan, Jupiter, and Uranus, largely because methane (or its photochemical products) plays a similar role in these atmospheres to terrestrial ozone (de Pater & Lissauer, 2001; pp. 94–96). It is likely that methane played a similar role on the early Earth (Pavlov *et al.*, 2001 and see later). If the early atmosphere were enriched in CO_2 (Kasting *et al.*, 1984), cold stratospheric temperatures would severely limit the abiotic production of oxygen (Kasting & Ackerman, 1986). H_2O photodissociation and H escape might have provided oxygen to the Hadean Earth, as water vapor can reach the upper atmosphere during magma ocean conditions (Kasting, 1988), subsequent to giant impacts. Focusing on the Archean forward, we ignore the photolysis of H_2O and CO_2 as an oxidizing source.

Oxygen readily reacts with reductants. Whether oxygen liberated by organic burial accumulates in the atmosphere or not depends entirely on the kinetics of its chemical loss to reductants in the atmosphere, ocean and on the land surface (Walker *et al.*, 1983). In its most general formulation, we describe the evolution of free oxygen on geological timescales by the interplay between its sources (F_{SOURCE}) and sinks (F_{SINK}), i.e.

$$\frac{d}{dt}[O_2] = F_{SOURCE} - F_{SINK} = (F_B + F_E) - (F_V + F_M + F_W) \quad (2)$$

where $[O_2]$ is the total reservoir of atmospheric dioxygen, which we quantify in units of teramoles (where 1 Tmol = 10^{12} mol), although we sometimes convert to bars for graphic display purposes. All source and sink fluxes are described in units of Tmol year^{-1}. We split F_{SOURCE} into F_B, the flux of oxygen due to organic carbon burial, and F_E, the flux of oxygen to the Earth as a whole due to hydrogen escape. The oxygen sinks F_V and F_M represent reducing gases (i.e. H_2, H_2S, CO, CH_4) from volcanic/hydrothermal and metamorphic/geothermal processes, respectively, while F_W is the oxygen sink due to oxidative weathering of continental rocks. Equation 2 is illustrated by considering fluxes in and out of the atmosphere/ocean/biosphere ('AOB') box in Fig. 2, our first-order conceptualization of the Earth system.

The only way that oxygen levels could have changed with time is if the source or sink terms on the right hand side of equation 2 change with time. Clearly, for oxygen to rise, it requires that $F_{SOURCE} > F_{SINK}$ at some time. A constant oxygen level in the atmosphere is achieved when the time derivative term is zero and $F_{SOURCE} = F_{SINK}$. Because equation 2 is general, these aspects of oxygen evolution are true irrespective of any particular model. If F_{SOURCE}, F_{SINK} or both terms are functions of the oxygen concentration in the atmosphere, in principle, we can solve equation 2 and determine Earth's oxygen history. This then, is the essence of the model that we construct in this paper.

We now summarize various previous qualitative attempts at describing the evolution of atmospheric oxygen in terms of various changes in the long term sources and sinks.

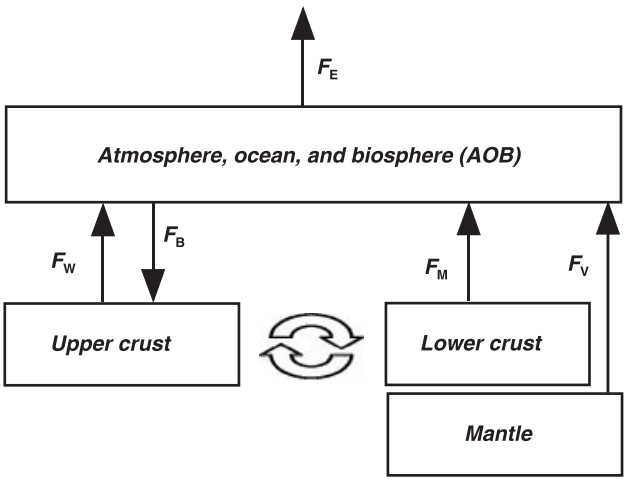

Fig. 2 A schematic of our box model. The arrows represent fluxes of reducing material . Arrows leaving a box thus represent oxidizing processes, so equation 2 for the evolution of oxygen is obtained by subtracting the incoming reductant fluxes from the outgoing reductant fluxes. The unfilled arrows represent crustal mixing due to erosion, uplift, and tectonics.

2.2 Increase in the O_2 source

One class of models discussed in the literature argues that increases in atmospheric O_2 are directly related to changes in the source flux.

2.2.1 Step changes

As nearly all free oxygen on Earth derives from oxygenic photosynthesis, it is reasonable to assume that the evolution of this metabolic pathway was the fundamental driver in the timing of the rise in planetary O_2 levels. Indeed, some have argued that oxygen appeared in the atmosphere as soon as oxygenic photosynthesis evolved (Ohmoto, 1996; Kopp *et al.*, 2005). However, multiple lines of evidence indicate that cyanobacteria evolved significantly prior to the rise of oxygen, which effectively rule out this hypothesis. The most direct evidence for the existence of ancient cyanobacteria occurs in the 2.7 Ga Pilbara Craton, in which 2-alpha-methylhopanes were found (Brocks *et al.*, 1999, 2003). The only known organisms that produce long-chain (i.e. >C31) varieties of these particular molecules are certain cyanobacteria (Brocks *et al.*, 2003; Summons & Brocks, 2004). In addition, C28–C30 steranes were found in the same deposit as the 2-alpha-methylhopanes. Such steranes are the diagenetic derivatives of sterols. Sterols in the modern biosphere are found in eukaryotes and synthesized in a pathway that requires free molecular oxygen (Summons *et al.*, 2006). No bacteria are known to synthesize C28–C30 sterols and archea do not synthesize sterols at all. The simultaneous codetection of long chain (>C31) 2-alpha-methylhopanes with eukaryotic sterols is a robust biosignature for organisms capable of oxygenic

photosynthesis, and is strongly suggestive evidence for the existence of cyanobacteria at 2.7 Ga.

Moreover, the detection of cyanobacterial biomarkers and steranes prior to the rise of oxygen is not one isolated result. Using a rigorous procedure, cyanobacterial biomarkers and diverse steranes have been detected in fluid inclusions in the 2.45 Ga Matinenda Formation at Elliot Lake, Canada (Dutkiewicz *et al.*, 2006), which is a uraniferous sandstone deposited in a reduced environment prior to both the rise of oxygen (Bekker *et al.*, 2004) and the Huronian glaciations (Young *et al.*, 2001). It seems likely that as more biomarker analyses are conducted in the Archean, further evidence will accumulate for the origin of oxygenic photosynthesis prior to the oxygenation of the atmosphere. Additional evidence to support the early evolution of oxygenic photosynthesis (including nonsulfatic stromatolites, isotopic indicators of the presence of methanotrophs, and the isotopic records of C, S, U, and Pb) have been recently reviewed (Canfield, 2005; Catling & Claire, 2005; Holland, 2006). Taken together, the data indicate an evolution of oxygenic photosynthesis at least 0.4 Gyr and perhaps as much as 1.3 Gyr prior to the GOE. Given the ubiquity of the substrate (CO_2, H_2O and photons), oxygenic photosynthesizers probably radiated quickly and became dominant players in the planetary ecosystem (Des Marais, 2000), as they are today, limited only by the availability of trace nutrients such as phosphorus and nitrogen (Tyrell, 1999). As a result, any theory for the rise in atmospheric oxygen levels must contain a mechanism by which reducing conditions can be maintained even in the presence of a substantial flux of organic carbon burial and associated net O_2 production prior to 2.4 Ga.

Before further discussion, we acknowledge that alternate views regarding whether or not the GOE took place do exist, albeit among a minority of researchers. Ohmoto and colleagues have argued that the geological record preserves localized evidence of significant oxidation prior to 2.4 Ga (e.g. Ohmoto (1996)), but also propose a much earlier oxygenation of Earth's atmosphere. Analyses that show the presence of mass-independent fractionation (MIF) of sulfur isotopes in Archean rocks (Farquhar *et al.*, 2000; Farquhar & Wing, 2003; Ono *et al.*, 2003; Zahnle *et al.*, 2006) provide to many observers convincing evidence that the Archean atmosphere was globally weakly reducing. Local oxygen 'oases' likely occurred in surface waters as the result of cyanobacterial activity and the limitation on the diffusion rate of oxygen from the surface ocean into the atmosphere (Kasting, 1992). In this paper, we accept the consensus view that a major change in oxygen concentrations in the atmosphere occurred at ~2.4 Ga.

2.2.2 Cumulative burial of organic material

A small fraction (0.1–0.2%) of photosynthetically produced organic carbon escapes re-oxidation in the water column and the upper oxic layer of sediments (Betts & Holland, 1991; Field *et al.*, 1998), representing a net source of 10 ± 3 Tmol year^{-1} of free oxygen to the hydrosphere via equation 1 (Holland, 2002). Given the direct correlation between organic carbon burial and the production of free oxygen, many models exist that tie oxygen levels to putative changes in the global burial flux of organic carbon.

a) Disproportionation of CO_2

One historical line of argument arises from inspection of the bulk crustal rock record. Early compilations show an approximate correspondence between the total reservoirs of reduced sedimentary carbon and oxidized iron and sulfur (e.g. Ronov, 1983). Given this correspondence, one can imagine the 'history' of the Earth system as the reduction of volcanically produced CO_2 to organic carbon with the excess oxygen consumed in the conversion of ferrous to ferric iron and sulfides to sulfates (Walker, 1990b). This hypothesis relied on estimates of bulk crustal composition that predated the acceptance of plate tectonics and its influence on crustal production. Continents were assumed to be primary features of Earth, rather than formed from mantle-derived igneous rocks. Consequently, these early compilations ignored oxidized iron in the nonsedimentary components of Earth's crust. It is useful to think of the igneous and high-grade metamorphic rocks of Earth's crust as 'hard rocks' and sediments as 'soft rocks' (Sleep, 2005a). The inventory of excess oxygen in 'soft' rocks (i.e. sulfates and iron oxides in sediments) plus the atmosphere and ocean, is vastly outweighed by excess oxygen in 'hard' rocks. An excess inventory of $1000–2000 \times 10^{18}$ mol O_2 are observed in hard rocks and $\sim 300 \times 10^{18}$ mol O_2 in soft rocks (Catling *et al.*, 2001; Sleep, 2005a; Hayes & Waldbauer, 2006), nullifying the assumptions of the CO_2 disproportionation hypothesis. This hypothesis also has additional difficulties in that there is no compelling reason that oxygen should rise (or even exist) in the atmosphere at all.

b) Secular changes in the burial of organic carbon

Secular changes in the rate of organic carbon burial have been proposed to describe the history of atmospheric oxygen. Assuming the global carbon cycle is in steady state implies a mass balance for the ^{13}C and ^{12}C isotopes on timescales exceeding $\sim 10^5$ years, the residence time of oceanic carbon (Walker, 1990a). $\delta^{13}C$ is a measurement of the relative amount of ^{13}C to ^{12}C in a sample and is widely used as a palaeoindicator given its comparative resistance to diagenetic resetting (Schidlowski, 2001). $(\delta^{13}C = [(^{13}C/^{12}C)_{sample}/(^{13}C/^{12}C)_{standard} - 1] \times 1000$, is measured in parts per thousand (‰) against the international standard of a fossil marine carbonate, Vienna Peedee Belemnite (VPDB) (Coplen, 1994)). Mass balance is commonly expressed as $\delta^{13}C_{in} = \delta^{13}C_{out}$, where $\delta^{13}C_{in}$ is the average isotopic composition of all carbon input into the rapidly exchangeable 'AOB' reservoir, and $\delta^{13}C_{out}$ is the isotopic composition of all carbon removed from the AOB reservoir. ^{13}C and ^{12}C exit the global carbon cycle in either carbonates ($\delta^{13}C_{carb}$) or organic carbon ($\delta^{13}C_{org}$), so that

$$\delta^{13}C_{out} = \delta^{13}C_{carb}f_{carb} + \delta^{13}C_{org}f_{org} = \delta^{13}C_{carb} + f_{org}(\delta^{13}C_{org} - \delta^{13}C_{carb}) \quad (3)$$

where f_{org} is the fraction of carbon buried as organic matter, f_{carb} is the fraction of carbon buried as carbonates, and $f_{carb} + f_{org} = 1$. Over rock-cycle timescales, the mass weighted average $\delta^{13}C$ of the recycled input into the global carbon cycle must equal the input from the mantle (Hayes & Waldbauer, 2006). Diamonds from peridotite xenoliths throughout geological time have $\delta^{13}C$ values similar to that of the modern mantle (Pearson *et al.*, 2004) so we follow the traditional approach and adopt the average mantle value of $\delta^{13}C_{in} = \delta^{13}C_{out} \sim -6‰$ (Holser *et al.*, 1988), as calculated from a subset of mantle diamonds and mantle-derived basalts. Measurements of average $\delta^{13}C_{carb}$ for all geological eons are ~0‰ because the standard is itself a marine carbonate of typical isotopic composition (Schidlowski, 1988). Inserting these numbers into equation 3 along with the observed average difference between $\delta^{13}C_{org}$ and $\delta^{13}C_{carb}$ (~30‰ (Schidlowski, 1988)) provide the estimate that over most epochs of Earth's history, ~1/5 of the carbon input is buried as organic matter. Currently, there is no complete explanation for why carbon should separate out in 4 : 1 proportions in carbonate and organic carbon burial fluxes, despite the considerable changes in the structure of the biosphere over geological history, although the geochemical cycle of phosphorus appears to be crucial (Junge *et al.*, 1975; Ruttenberg, 2004).

A secular increase in f_{org} from 2.6 Ga onwards is suggested based on boxcar averaging of ancient $\delta^{13}C$ measurements (Des Marais *et al.*, 1992), but these results are influenced by choosing starting dates at the period of Earth's history with the most depleted $\delta^{13}C_{org}$ values. Methanotrophic recycling of organic carbon created by photosynthesizers has been implicated in the production of these anomalously low $\delta^{13}C_{org}$ values (Hayes, 1994; Hinrichs, 2002; Hayes & Waldbauer, 2006). Another recent model (Bjerrum & Canfield, 2004) also suggests that f_{org} increased from the mid-Archean forward by assuming significant loss of carbon to hydrothermal carbonates. While the process of hydrothermal carbonatization appears to be very important in quantitative treatments of the Archean carbon cycle (Sleep & Zahnle, 2001; Hayes & Waldbauer, 2006), the Bjerrum & Canfield (2004) model assumes a biologically pumped gradient in $\delta^{13}C$ between the surface ocean and seafloor but measurements of 3.46 Ga seafloor show no such gradient (Nakamura & Kato, 2004). Hayes & Waldbauer (2006) provide additional arguments against the secular evolution of f_{org} via an expanded version of equation 3 incorporating hydrothermal carbonatization and subduction zone processes, arguing that f_{org} is approximately constant throughout most of the Archean and Proterozoic.

A different, albeit less direct, hypothesis in this category involves continental growth rates. Two important processes may be tied to the total volume of continental crust – organic carbon burial on the continental shelves and phosphorus weathering from continental rocks. Previous numeric models that incorporated continental growth have assumed pO_2 proportional to carbon burial and carbon burial proportional to continental area, and hence show the rise of O_2 as a direct product of continental growth (Godderis & Veizer, 2000), a result that is prescriptive rather than descriptive. Due to many measurement difficulties, the time evolution of the growth of the continents remains a field of inquiry, although most models predict that at least 70% of current continental volume was in place by 2 Ga (Rogers & Santosh, 2004; p. 48).

c) A pulse in organic carbon burial

Karhu & Holland (1996) hypothesize that a pulse in organic carbon burial might have caused the rise in atmospheric oxygen. This was based on their interpretation of a prolonged 300 Myr positive excursion in $\delta^{13}C_{carb}$, which, when coupled with a steady state interpretation of the global carbon cycle, implies that 11–22 times the present amount of atmospheric oxygen could have been generated (Karhu & Holland, 1996). The early Palaeoproterozoic sedimentary record remains incomplete, but the required organic carbon associated with such a burial pulse appears to be missing (Melezhik *et al.*, 1999; Aharon, 2005). In addition, the peak of the isotope excursions occurred at 2.2 Ga, well after the initial rise in O_2 levels before 2.32 Ga, as evidenced by disappearance of MIF S (Bekker *et al.*, 2004), indicating that the carbon isotope excursion is more likely an effect rather than a cause (Holland, 2002; Hayes & Waldbauer, 2006). Finer resolution data reveal the 'Lomagundi event' as several spikes of $\delta^{13}C$ in marine carbonates coupled with return to low values (Melezhik *et al.*, 1999, 2005; Lindsay & Brasier, 2002), which argues for more complexity than a single pulse in the carbon burial. Hayes & Waldbauer (2006) argue that the $\delta^{13}C$ excursions may represent unusual times in Earth's history when the diagenetic effects of methanogenesis were preserved.

2.3 A decreasing sink for O_2

Estimates of Archean global gross productivity are necessarily difficult to quantify but net production of O_2 via organic carbon burial is constrained by the record of carbon isotopes. Given the approximate stasis in global carbon isotopes (Schidlowski, 1988) and the approximately constant 0.5 wt% of organic carbon in sediments over geological time (Holland, 1984; pp. 352–364), many researchers conclude that once oxygenic photosynthesis evolved, net oxygen production since the late Archean has been approximately constant relative to the total carbon flux in and out of the atmosphere–ocean system (Des Marais, 2000). This interpretation would leave a secular decrease in oxygen destruction as a plausible mechanism for explaining the rise in oxygen.

2.3.1 Decreasing sink from volcanic outgassing

Simply decreasing the total flux of volcanic gases as the Earth cooled (Christensen, 1985) is not sufficient to decrease the O_2

sink. Increased volcanic outgassing would have injected proportionally more CO_2 into the atmosphere in addition to any enhancement in reducing gases. But since ~20% of CO_2 has been buried as organic matter over geological time (see the previous section), oxygen production due to enhanced organic burial would counteract any enhancement in the reductant sink. To see this, consider a hypothetical volcano releasing 5 Tmol year^{-1} of CO_2 and 1 Tmol year^{-1} 'O_2 equivalent reductants' (i.e. as H_2, CH_4, CO, etc.). This toy volcano does not change the steady state level of atmospheric O_2 if 1/5 of the CO_2 is buried as organic carbon, releasing 1 Tmol year^{-1} of O_2. This conclusion is unchanged if the total volcanic outgassing rate increases – the only way to affect the net redox balance is via a change in the ratio of reducing gases to CO_2.

Realizing this, Kasting and colleagues developed a model invoking decreasing proportions of reducing to neutral gases (generally described as the H_2/CO_2 ratio) emanating from Earth's mantle as the mantle progressively oxidizes with time (Kasting *et al.*, 1993; Kump *et al.*, 2001). In this model, hydrogen escape is balanced by input of reductants from the mantle, so there is no net oxidation of the continents. This model can be formalized by a simplified version of equation 2 in which

$$\frac{d}{dt}[O_2] = F_B - F_{V,KK} - F_W \quad (4)$$

where $F_{V,KK}$ indicates the volcanic parameterization in the manner of Kasting *et al.* (1993) and Kump *et al.* (2001) which for our purposes are volcanic gases that can consume atmospheric O_2. Walker (1977) argues that at extremely low O_2 levels oxidative weathering will be negligible, at moderate O_2 the rate of oxidative weathering should be proportional to oxygen levels, and at high O_2 levels oxidative weathering should once again become independent of O_2 levels (Walker, 1977; pp. 103–105). A function that fits this behaviour is $F_W = k_W * [O_2]^\beta$, where k_W is a constant. We adopt a constant $\beta = 1/3$ using an analogue of CO_2 weathering behaviour where β has been calibrated (Holland, 1978; p. 20), because this exponent probably captures the first-order behaviour expected for O_2. Later we explore the sensitivity to changing the exact value of β in numerical computations. This general formulation of oxidative weathering is supported by the evolution in the ferric/ferrous ratio of shales, which show a dramatic increase between 2.3 and 2.1 Ga (Holland, 2006).

For a heuristic estimate below, we approximate the oxidative weathering flux in the 'moderate O_2' regime by $F_W = C * [O_2]$, where C is a proportionality constant. In steady state, the time derivative of the oxygen reservoir in the atmosphere must be zero, i.e. $d[O_2]/dt = 0$. Substituting for F_W and assuming steady state in equation 4 yields

$$[O_2] = (F_B - F_{V,KK})/C \quad (5)$$

In this fashion, the rise of O_2 can be explained by decreasing the magnitude of $F_{V,KK}$ relative to F_B (assumed constant). When $F_{V,KK}$ exceeds F_B, the oxygen concentration in equation 5 is negative and the equation no longer holds. In that case, the atmospheric redox state is dominated by reducing gases.

Measurements of the redox-sensitive trace elements Cr, V, and Sc in basalts (Canil, 1999; Delano, 2001; Li & Lee, 2004) have cast doubt on models that invoke redox evolution of the mantle. Because Sc and V partition similarly apart from their redox sensitivity, Li & Lee (2004) have shown using V/Sc ratios that Archean mantle differed in oxygen fugacity from the modern mantle by no more that 0.3 $\log_{10}$ units, an amount insufficient to promote a reduced atmosphere (Holland, 2002). Rather than a smooth decline in volcanic reductants, some workers argue for a step change decrease in the reducing power from the mantle at ~2.4 Ga (Kump *et al.*, 2001; Barley *et al.*, 2005). This model speculates that the entire mantle overturns, bringing oxidized material from the core mantle boundary to the upper mantle. The V/Sc data for Archean and modern basalts reveal nearly identical oxygen fugacity and spread, so any argument that invokes mantle redox evolution requires that the entire signal from changes in mantle fugacity are completely buried in the noise. Given these arguments, we concur with Li & Lee (2004) that the oxygen fugacity of the mantle is unlikely to be the major driver of atmospheric O_2 levels.

A further refinement of the declining volcanic flux model involves an enhanced Archean flux of both H_2 and hydrothermal cations (Fe^{2+}) venting from mid-ocean ridges (Kump & Seyfried, 2005). This process perhaps avoids the constraint on mantle redox evolution. Conceptually, reduced hydrothermal/geothermal cations behave as effective reductant contributions to F_V or F_M through schematic reactions such as $2Fe^{2+} + 3H_2O = Fe_2O_3 + 4H^+ + H_2$. Kump & Seyfried (2005) argue that lower oceanic sulfate levels and shallow mid-ocean ridges will increase the Fe^{2+}/H_2S ratio of vent fluids, allowing for an iron-rich deep ocean conducive to the deposition of banded iron formation and supportive of vigorous methanogenesis. This process could certainly be important on the Archean earth, but we are unable to evaluate it further as the authors do not present quantitative estimates of the magnitude of the enhanced fluxes.

2.3.2 *Decreasing sink of metamorphic gases*

Catling *et al.* (2001) suggest evolution in the redox state of metamorphic gases derived from Earth's crust. The crustal reservoir evolves independently of redox state of the mantle, so the Cr, V, and Sc data do not bear on it. This model requires high rates of hydrogen escape early in Earth history relative to the present day, which drives a redox change of the crust and mantle. The model allows for mantle redox change within the small limits constrained by observations but assumes that the mantle oxidation state is strongly buffered. The rise of oxygen is explained by the progressive oxidation of the continental crust by hydrogen escape, which in turn reduces the proportions of reductants from crustally derived metamorphic gases, decreasing the sink for O_2. The primary drawback of this

model is the lack of a general theory for the evolution of metamorphic gases, and the absence of geological proxies for palaeo CH_4 levels.

Holland has a somewhat similar conceptual model, which emphasizes low temperature hydrothermal/geothermal sources of reductants from the seafloor and considers the effects of the sulfur cycle on the oxidation state of the atmosphere (Holland, 2002). He argues that Archean sulfate-poor oceans (Canfield *et al.*, 2000) would have led to slower sulfur cycling, and hence volcanic and metamorphic gases with a lower $\Sigma S/H_2O$ ratio. Excess hydrogen could have reduced all SO_2 to pyrite without the corresponding O_2 source that occurs at higher $\Sigma S/H_2O$ levels from pyrite burial. Testing this hypothesis lies beyond the scope of this paper, as it would require incorporation of the sulfur cycle into our biogeochemical model. However, the Catling *et al.* (2001) model is qualitatively similar to Holland (2002) in that hydrothermal/geothermal fluids can become more oxidizing, with CH_4 derived from excess H_2 via biological activity. Indeed, there are good reasons to believe that a significant concentration (>100 ppmv) of H_2 is unlikely to exist in the Archean atmosphere because it can serve as a substrate for anoxygenic photosynthesis and methanogenesis, which together recycle the hydrogen to organic matter and then methane. In laboratory experiments, methanogens draw down H_2 to produce methane until they reach a thermodynamic limit at ~0.01% H_2 (Kral *et al.*, 1998). Biomarkers and carbon isotopes suggest that methanogens were present in the Archean (Hayes, 1994; Hinrichs, 2002; Brocks *et al.*, 2003). In addition, methanogens are strictly anaerobic with a tendency toward thermophily, which suggests that they are evolutionarily ancient (Teske *et al.*, 2003). Thus, methanogens likely would have converted any excess atmospheric H_2 into methane (Kasting *et al.*, 2001; Kharecha *et al.*, 2005).

The purpose of this paper is to extend the above qualitative descriptions of the rise of oxygen to the quantitative realm, and to obtain a fully self-consistent mathematical framework for the redox evolution of Earth's atmosphere and lithosphere. Consequently, we continue the discussion by considering analytical and numerical viewpoints in the following sections.

3. GLOBAL SOURCES VS. SINKS OF REDUCTANTS

We have introduced the concept of the evolution of atmospheric O_2 as interplay between its sources and sinks, an idea that we now extend by expanding the RHS of equation 2. For the purposes of this paper, we must consider the effect of reductant fluxes on both the oxygen level and the reduced components of the atmosphere. We represent the reduced gas component of the atmosphere as $[CH_4]$ which we take as a proxy for all reduced hydrogen-containing gases. In this way, for example, we treat H_2 as $1/2$ of a $[CH_4]$ redox equivalent (i.e. via net atmospheric or metabolic reactions like $CO_2 + 2H_2 \rightarrow CH_4 + O_2$).

3.1 Biosphere

For clarity, we restrict our scope to modelling the Earth after the advent of oxygenic photosynthesis, estimated by various workers as >2.5–3.7 Ga (see previous discussion). Given sufficient nutrient availability, oxygenic photosynthesis probably dominated global productivity once it evolved because cyanobacteria can extract H from ubiquitous water rather than relying on spatially scarce geological sources of reductant (Des Marais, 2000). Consequently, we consider photosynthesis as our key source of organic matter whose subsequent processing could potentially affect gas fluxes to the atmosphere. Other organic generation, e.g. by high temperature life, is unlikely to significantly affect gas fluxes once oxygenic photosynthesis has emerged. Considering changes in Earth's redox evolution over long time periods allows us to examine net redox fluxes and not gross cycles of all redox changes within all microbial communities, greatly simplifying our mathematical treatment of the biosphere. Heterotrophy (including respiration), microbial Fe-oxidation/reduction, and other detailed microbial redox interactions result in zero-sum redox exchanges that do not contribute directly to redox change in the atmosphere. For example, respiration consumes ~99.9% of photosynthesized organic matter, so that we need only consider the long-term O_2 flux associated with the leak of organic matter into buried sediments rather than the gross photosynthesis–respiration cycle. Furthermore, the organic burial rate is constrained by the carbon isotope record so that it is not necessary to consider all ancient pathways of remineralization in order to deduce organic carbon burial and associated O_2 production. Similarly, we ignore the gross microbial iron oxidation–reduction cycle, including only the net effect on the oxygen cycle, which is evident in the evolution of the ferric/ferrous ratio in shales (Holland, 2006).

We do not have inferential geochemistry for biogenic CH_4 or H_2 fluxes to the ancient atmosphere. Our approach in these cases is to impose gas fluxes that are redox balanced with corresponding production of O_2 (which may, of course, create its surrogates (Fe^{3+}, SO_4, etc.)), assuming that the metabolic source for any organic matter derives from photosynthesis. Such gas fluxes can be varied to assess model sensitivity, bounded by what is known about modern fluxes subject to changing physical conditions such as nutrient limitation or substrate availability. In essence, such variations parametrically take into account possible scenarios with different degrees of heterotrophy, anaerobic CH_4 oxidation, etc., relative to methanogenesis (Kharecha *et al.*, 2005). We begin our expansion of equation 2 to include the quantitatively important biospheric redox terms by expanding on F_B, the organic carbon burial term.

Information on organic burial, F_B, comes from the carbon isotope record that suggests that ~20% of the carbon coming into the system was buried as organic carbon during most of Earth's history (Schidlowski, 1988). Today, F_B ~10 Tmol O_2 $year^{-1}$ (Holland, 2002). If the amount of carbon entering

the Archean atmosphere–ocean system was similar to today, C isotopes roughly constrain F_B to be similar to today. To first-order then, we assume oxygen production due to organic burial has remained constant (relative to the influx of carbon to the atmosphere–ocean system) since the evolution of oxygenic photosynthesis. On the modern Earth, photosynthetically produced organic carbon is used by microbes to reduce sulfate to pyrite, so that when such pyrite is buried, oxygen is effectively liberated to a degree that is quantitatively significant (Holland, 2002; Berner, 2004; pp. 101–103). However, in the Archean oceans, the lack of significant sulfur isotope fractionation implies that sulfate levels were low (Canfield *et al.*, 2000; Habicht *et al.*, 2002). Consequently, to keep our early Earth model simple, we assume that the F_{SOURCE} term was dominated by the burial flux of organic carbon (F_B) for the Archean.

The net effect of oxygenic photosynthesis is the slow flux of oxygen via organic carbon burial discussed previously, but alternate fates exist for photosynthetically produced organic carbon. The important fate to consider for our model is methanogenesis because this process releases a redox-sensitive gas to the atmosphere. Rather than respiration or burial, a microbial community of fermenters and methanogens can further processes organic carbon via the following net redox reaction:

$$2CH_2O \rightarrow CH_4 + CO_2 \quad (6)$$

The net effect of methanogenic recycling of photosynthetically produced organic carbon is found by summing two times equation 1 and equation 6, yielding:

$$CO_2 + 2H_2O \rightarrow CH_4 + 2O_2 \quad (7)$$

Thus, the combination of oxygenic photosynthesis and methanogenesis produces O_2 and CH_4 in a 2 : 1 ratio. Methane-oxidizing bacteria (methanotrophs) live off the reverse reaction of equation 7, although their habitat is limited to regions where both methane and oxygen can coexist, such as the anoxic/oxic boundary layers at the sediment/water interface. 'Anaerobic' methane oxidation (AMO) occurs by a consortium of organisms, but all known pathways require either SO_4^{2-} (Valentine, 2002), or NO_3^- (Raghoebarsing *et al.*, 2006). The quantitatively significant source of oceanic SO_4^{2-} is O_2-dependent oxidative weathering (Holland, 1978; pp. 46–49; Walker & Brimblecombe, 1985), and the lack of $\delta^{34}S$ fractionation in sediments argues for low sulfate levels in the Archean oceans (Canfield *et al.*, 2000; Habicht *et al.*, 2002). Nitrogen fixation ($N_2 \rightarrow NH_4^+$) is thought to be genetically ancient, but O_2 is required to further oxidize the ammonia to nitrate, so NH_4^+ was likely the dominant nitrogen species in Archean oceans prior to the rise in oxygen (Beaumont & Robert, 1999; Berman-Frank *et al.*, 2003). For simplicity, we assume Archean AMO to be limited by sulfate and nitrate availability, allowing for a greater CH_4 flux, although both of these pathways may have been important in the transitional atmosphere.

The global occurrence of kerogens strongly depleted in ^{13}C at ~2.8–2.5 Ga is likely evidence for isotopically light CH_4 >20 ppmv, generated by methanogens and incorporated into methanotrophs (Hayes, 1994). Today, ~4% of organic carbon from total gross productivity (~10^4 Tmol year^{-1}) is estimated to undergo anaerobic conversion into CH_4 (Watson *et al.*, 1978). However, upward diffusion of CH_4 from seafloor sediments is almost totally cancelled by SO_4^{2-} reduction (i.e. AMO) at the CH_4-SO_4^{2-} transition zone (D'Hondt *et al.*, 2002). This means that an enormous oceanic flux of CH_4 never reaches the modern atmosphere. Unlike today, there was very little sulfate in the Archean oceans (Habicht *et al.*, 2002), which were deeply anoxic as evidenced by the transport of ferrous iron (Holland, 1984; pp. 379–388). Thus, it is probable that the Archean ocean was a much larger source of CH_4 than today. If all the CH_4 escaped today without oxidation, ~200 Tmol CH_4 year^{-1} ($4\% \times 10^4/2$) would be released to the air via equation 6, with the net effect of 400 Tmol year^{-1} of O_2-consuming reducing equivalents. The Archean CH_4 flux could have been similar or greater due to the lower rates of aerobic remineralization in anoxic waters. In the Black Sea, the burial efficiency is ~10 times higher than in the modern oceans (Arthur *et al.*, 1994) and if there were negligible sulfate, the CH_4 flux from the Black Sea to the air would be ~70 times greater than present (Reeburgh *et al.*, 1991). To first order, we assume that Archean CH_4 was derived from photosynthetized organics so that O_2 and CH_4 were generated in stoichiometric 2 : 1 abundance via equation 7. Today's net CH_4 flux of ~30 Tmol CH_4 year^{-1} (Watson *et al.*, 1990) and the numbers quoted above bound a reasonable range of probable CH_4 fluxes.

We note that laboratory experiments with microbial mats conducted in the modern oxic atmosphere but at low sulfate levels show only modest remineralization (~0.4%) by methanogenesis and a methane flux increase by only a factor of ~10 (Bebout *et al.*, 2002). As described above, anoxic seafloor sediments could produce a very significant Archean methane flux, and are not constrained by these mat experiments. Similarly, although large H_2 fluxes may also emanate from mats (Hoehler *et al.*, 2001), H_2 is unlikely to have built up in the atmosphere because of its tendency to be converted to less metabolically desirable methane (Kral *et al.*, 1998; Kasting *et al.*, 2001; Kharecha *et al.*, 2005), as discussed previously. In our model, for simplicity, biological H_2 fluxes are effectively carried in the CH_4 flux budget.

3.2 Effective reaction of CH_4 and O_2

We have chosen to use a single reservoir for the entire AOB for our box model (see Section 2 and Fig. 2), so we do not separate aqueous biological chemistry from atmospheric chemistry when considering the mutual annihilation of CH_4 and O_2, which is a simplification. It would be highly desirable to add methanotrophic destruction of CH_4 and O_2 (or SO_4^{2-}), but

our initial goal is to study the simplest system with a minimum number of tunable parameters. In essence, we assume aqueous methanotrophy is relatively minor in the low sulfate Archean ocean and what does occur is a closed cycle that need not concern us. Thus, we parameterize the mutual annihilation of CH_4 by O_2 solely from atmospheric destruction, and apply the parameterization to the entire AOB reservoir. We define an effective rate constant k_{eff}, with units of $Tmol^{-1}$ $year^{-1}$, via:

$$F_{CH4} = k_{eff}[O_2][CH_4] \quad (8)$$

where F_{CH4} is the CH_4 flux into the atmosphere, $[O_2]$ and $[CH_4]$ are the global atmospheric inventories in Tmol, and k_{eff} is itself a function of the O_2 and CH_4 levels. The atmospheric annihilation of O_2 by CH_4 is the net sum of many photochemical reactions that are initiated with a photochemical reaction involving an attack on a methane molecule by the OH radical ($OH + CH_4 \rightarrow CH_3 + H_2O$). In the modern atmosphere, away from polluted areas, OH is produced in the troposphere by a series of steps beginning with the photochemical destruction of tropospheric O_3 (Finlayson-Pitts *et al.*, 2000, pp. 179–180):

$$O_3 + h\nu(\lambda \leq 336\,nm) \rightarrow O(^1D) + O_2$$
$$O(^1D) + H_2O \rightarrow 2OH$$

where $O(^1D)$ is an electronically excited oxygen atom. The tropospheric ozone itself derives from the collision of an oxygen molecule with an oxygen atom and a third body, and so depends on the presence of an oxic atmosphere. Prior to the rise of O_2, photochemical models show limited OH abundances (Kasting, 1979). Although shortwave ultraviolet reaches the lower atmosphere in the absence of a stratospheric ozone layer and can photolyse water vapor directly, the photolysis products rapidly recombine given that O_2 molecules are not available to rapidly remove the H produced in photolysis. The net result is that the anoxic Archean atmosphere allows a steady-state CH_4 concentration that is much larger than today, given a plausible flux of methane (Pavlov *et al.*, 2001). These same photochemical models show that O_3 levels rise nonlinearly with O_2 so that significant OH is produced even at intermediate oxygen levels (Kasting & Donahue, 1980). This positive feedback on CH_4 destruction with rising levels of O_2 leads to a prediction of a geologically quick transition between O_2- and CH_4-dominated atmospheres.

In any regard, $k_{eff} = k_{eff}(O_2,CH_4)$ is a complicated function. In the modern atmosphere, we can compute $k_{eff} = 3 \times 10^{-9}$ $Tmol^{-1}$ $year^{-1}$ from a (net) CH_4 flux of 33 Tmol $year^{-1}$ (Houghton, 1994) into an atmosphere with 21% O_2 and 1.7 ppm CH_4. In an anoxic atmosphere, the multiple competing processes sketched above necessitate a numerical solution. We used the photochemical model of (Zahnle *et al.*, 2006) to compute k_{eff} in 1372 steady-state atmospheres with fixed O_2 surface mixing ratios ranging from 10^{-14} to 10^{-1} bar and fixed CH_4 levels from 10^{-6} to 4×10^{-3} bar. CO_2 was fixed at 10^{-2} bar and the upper bound on CH_4 levels was chosen to keep the CH_4/CO_2 ratio <0.5, thus avoiding the regime of particulate chemistry and photochemical smog (Pavlov *et al.*, 2001). Figure 3 shows some of our computed values of k_{eff} as function of CH_4 and O_2.

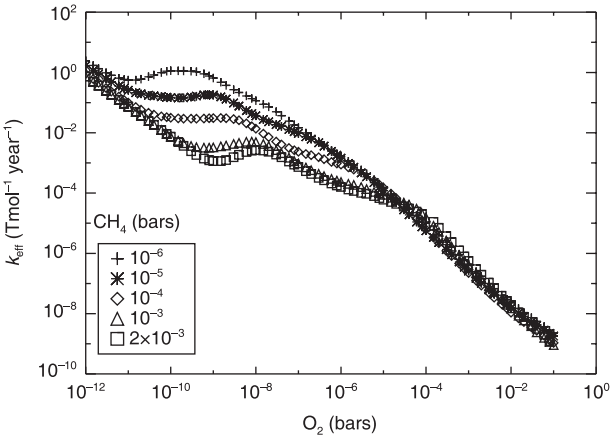

Fig. 3 Plots of $k_{eff}(O_2,CH_4)$ vs. O_2, as computed using the photochemical model of Zahnle *et al*. (2006). In the biogeochemical model, k_{eff} values were computed from a logarithmic weighting of the four grid points that bracket the given $[CH_4,O_2]$ pair. CH_4 values outside the computed limits were taken to be the limiting value.

3.3 Hydrogen escape

The final item to discuss is the calculation of the rate that hydrogen escapes to space from an anoxic atmosphere so we can quantify its effect on the redox evolution of the Earth system. As previously discussed, the permanent removal of H to space acts to irreversibly oxidize the reservoir from which the H originated. H escapes the planet by a combination of thermal and nonthermal processes acting high in the atmosphere (Hunten & Donahue, 1976; Hunten, 1990). According to this model, verified for the modern atmosphere by satellite and *in situ* measurements (Hunten & Donahue, 1976), the escape of H atoms is limited by the rate at which H atoms can make their way to the upper atmosphere, with two significant bottlenecks. First, hydrogen contributed from the ultraviolet decomposition of water vapor is throttled by the condensation of water vapor in the upper troposphere (see Section 2). Second, hydrogen that reaches the homopause then has to diffuse slowly to reach the exosphere. (Below the homopause (about 100 km altitude), the atmosphere is well mixed by turbulence; above the homopause atmospheric gases separate out according to their mass by diffusion and the atmospheric composition changes.) The ultimate bottleneck lies in the upward transfer of hydrogen (in all its forms) from the region above the tropospheric cold-trap. Despite the complexities of atmospheric photochemistry and dynamics, the numerical representation of hydrogen escape simplifies to a form proportional to the mixing ratios (f) of H-bearing

compounds above the cold-trap in the upper troposphere (Walker, 1977; pp. 157–163). For a hydrogen escape rate Φ, expressed in units of H_2 molecules cm^{-2} s^{-1}, we can write

$$\Phi = k_e f_{TOTAL} = k_e(0.5f_H + f_{H_2} + f_{H_2O} + 2f_{CH_4} + f_{H_2S} + \ldots) \quad (9)$$

where f_{TOTAL} is the total hydrogen mixing ratio, composed of the sum of the mixing ratios (f) of H_2, H_2O, CH_4, HCN, NH_3 and any other H-bearing gases that exist above the cold trap in the tropopause, weighted by the amount of hydrogen that they contain. In equation 9 above, we have described the hydrogen in terms of H_2 equivalents, although, depending on thermospheric conditions, hydrogen can also escape in atomic form. The numerical constant in equation 9 is an average diffusion constant for H and H_2 divided by an atmospheric scale height and to a reasonable approximation is given by $k_c = 2.5 \times 10^{13}$ H_2 molecules cm^{-2} s^{-1} (Walker, 1977; p. 164).

In our model, fluxes are expressed in teramoles per year, which demands some numerical conversion. Given that the area of the Earth is 5.1×10^{18} cm^2, we have a hydrogen escape flux as follows:

$$\begin{aligned}\Phi &= \left[\frac{(2.5\times10^{13}\,\text{molecules}\,\text{cm}^{-2}\,\text{s}^{-1})(3.15\times10^{7}\,\text{s}\,\text{yr}^{-1})(5.1\times10^{18}\,\text{cm}^2)}{(6.02\times10^{23}\,\text{molecules}\,\text{mol}^{-1})(10^{12}\,\text{mol}\,\text{Tmol}^{-1})}\right] \\ &\times f_{TOTAL} \\ &= 6680 f_{TOTAL}\ (\text{Tmol}\,H_2\,\text{yr}^{-1}) \\ &= 3340 f_{TOTAL}\ (\text{Tmol}\,O_2\,\text{yr}^{-1})\end{aligned} \quad (10)$$

We express all reductant gas fluxes as O_2-consuming equivalents, so the stoichiometry of $H_2 + 0.5O_2 = H_2O$ dictates that the redox flux in the second equality above must be divided by 2. In addition, we work with global atmospheric reservoir concentrations of teramoles rather than mixing ratios, which demands further numerical conversion for the f_{TOTAL} term, as follows. Assuming a 1 bar N_2 atmosphere with ζ bars of CH_4, the conversion factor between a Tmol of methane and a bar of methane is given by:

$$\begin{aligned}&\frac{(\text{column mass of air})\times(\text{area of Earth})}{\text{mean molar mass of air}} \\ &= \frac{(10^5\ \text{Pa}/9.81\,\text{m}\,\text{s}^{-2})\times(5.1\times10^{14}\,\text{m}^2)}{\left(\frac{0.028\times1+0.016\times\zeta}{1+\zeta}\,\text{kg}\,\text{mol}^{-1}\right)(10^{12}\,\text{mol}\,\text{Tmol}^{-1})} \\ &= 1.8\times10^{8}\ \text{Tmol}\,CH_4\,\text{bar}^{-1}\end{aligned} \quad (11)$$

which holds over the CH_4 range from $\zeta = 10^{-6}$–10^{-2}. The simplification of a 1 bar N_2 atmosphere is justified by the near-equivalent molecular weights of O_2 and N_2.

In our model, $[CH_4]$ includes all H-bearing compounds, so we use a first-order simplification of $f_{TOTAL} = 2[CH_4]$, where the factor of two arises because CH_4 contains the equivalent of two hydrogen molecules. Consequently, the diffusion-limited hydrogen escape parameterization in our model is expressed by substituting $f_{TOTAL} = 2[CH_4]$ into equation 10 and using the conversion factor of equation 11 to obtain:

$$F_E = k_{esc}[CH_4] \quad (12)$$

where $k_{esc} = 6680/1.8 \times 10^8 = 3.7 \times 10^{-5}$ (Tmol O_2 equivalents $year^{-1}$ (Tmol $CH_4)^{-1}$). Numerically, as 4 H atoms escape, we subtract a 'CH_4' from the methane reservoir of our model atmosphere. The dominant pathway for the remaining carbon atom (in both anoxic and oxic atmospheres) is to form CO_2 by a series of photochemical reactions, which acts as a sink for atmospheric O_2. Because of this, we must also subtract one O_2 redox equivalent from our atmospheric oxygen reservoir. However, since 1 mol of methane ordinarily consumes 2 mol of O_2 (the reverse of equation 7), the net effect is that the Earth system has gained an O_2 equivalent somewhere by hydrogen escape. Schematically, the overall effect is represented by $2O_2 + CH_4 \rightarrow CO_2 + 4H\uparrow_{space} + O_2$ (Catling *et al.*, 2001). Thus, planetary oxidation via hydrogen escape is indirect. The H that escapes was ultimately derived from an oxidized form of hydrogen (H_2O, OH in silicates, or hydrocarbons). The oxidation occurs in the original reservoir when the reduced H-bearing gas was released by oxidizing the surroundings, and is made permanent and irreversible if the resulting hydrogen atom escapes to space.

Reducing gas emanating from the solid Earth does not necessarily give rise to hydrogen escape directly but enables biogenic methane to serve as the source for hydrogen escape in the following subtle way. In the Archean, the reductant flux supplied by metamorphism or volcanism consumes oxygen that is co-generated with methane in 2 : 1 ratio via equation 7, so that the methane flux is no longer redox-balanced by oxygen equivalents. Consequently, methane is able to exist at higher abundance in the atmosphere and promote enhanced hydrogen escape according to equation 12.

There has been a recent suggestion (Tian *et al.*, 2005) that hydrogen escape on the prebiotic Earth might have been slower than that predicted via diffusion-limited H escape. As our paper deals with the consequences of a microbially inhabited Earth, the prebiotic atmosphere has no direct relevance to our argument. If, however, hydrogen escape was slow for a prolonged period on early Earth, the only way to quantitatively reconcile the observed surface oxidation is to preferentially subduct reduced materials to the mantle, a mechanism that runs counter to commonly expressed view of a gradual oxidation of the mantle and crust, and seems difficult in the face of large fluxes of ferric iron to the mantle (Lecuyer & Ricard, 1999). The conclusions of Tian *et al.* (2005) depend on an assumed cold thermospheric temperature and an assumed lack of importance for nonthermal escape. These assumptions have been called into question (Catling, 2006), and the results are inconsistent with other computations of a hot thermospheric temperature on early Earth (Kulikov *et al.*,

2006) and similar computations of hydrogen escape that allow atomic hydrogen to escape (Watson *et al.*, 1981). This complicated issue will certainly be the focus of continued research. Here, we retain the practice of most workers in the field using diffusion-limited parameterization to describe hydrogen escape from the Archean atmosphere.

3.4 Equations

The above arguments lead us to expand equation 2 into the following coupled time-dependent differential equations for the first-order redox evolution of the atmosphere:

$$\frac{d}{dt}[CH_4] = \phi_{CH4} - k_{eff}[O_2][CH_4] - k_{esc}[CH_4] \quad (13)$$

$$\frac{d}{dt}[O_2] = 2\phi_{CH4} - 2k_{eff}[O_2][CH_4] - k_{esc}[CH_4] + F_B - (F_V + F_M + F_W) \quad (14)$$

where ϕ_{CH4} is the flux from methanogenic microbial communities to the AOB, k_{eff} is the effective rate constant for the kinetic destruction of O_2 and CH_4 discussed in Section 3.2, $F_E = k_{esc}\,[CH_4]$ is subtracted from both equations as discussed in Section 3.3, and F_B, F_V, F_M, F_W are the reductant fluxes due to burial of organic carbon, volcanism, metamorphism, and oxidative weathering defined previously. It is important to remember that our fluxes are reductant fluxes, not total fluxes of all species, so that, for example, F_V is the total amount of reducing gases (i.e. H_2, H_2S, CH_4, CO, etc.) from volcanoes, and does not include the much more prevalent (by mole) gases (H_2O, CO_2) that do not consume O_2.

4 ANALYTIC SOLUTIONS OF EQUATIONS IN THE ANCIENT AND MODERN LIMITS

In steady state (i.e. $d[CH_4] = d[O_2] = 0$), we can eliminate ϕ_{CH4} between equations 13 and 14 to find that:

$$F_E + F_B = F_V + F_M + F_W \quad (15)$$

This balance allows an atmosphere to remain at a constant redox state, a condition that appears to mostly hold during the Phanerozoic as evidenced by the continuous presence of animals (Knoll & Carroll, 1999) and charcoal (Chaloner, 1989; Wildman *et al.*, 2004), although minor deviations have likely occurred (Berner *et al.*, 2003). The total hydrogen mixing ratio (as H_2 equivalents) above the modern tropopause is ~6 ppmv (Harries *et al.*, 1996), yielding a modern hydrogen escape flux of $F_{E,NOW} = 0.02$ Tmol O_2 year^{-1} via equation 10. Holland (2002) compiles the estimates we use to constrain modern values of the remaining parameters in equation 15. The rate of O_2 production during organic carbon sedimentation is estimated 10.0 ± 3.3 Tmol year^{-1} and the rate of O_2 use during weathering is estimated as 7.5 ± 2.5 Tmol year^{-1}, so we adopt the nominal values of $F_{B,NOW} = 10$ Tmol year^{-1} and $F_{W,NOW} = 7$ Tmol year^{-1} for the calculations below. Holland (2002) further estimates $F_{V,NOW} = 2.4 \pm 1.8$ Tmol year^{-1}, although two recent papers have suggested that this estimate may be too large by an order of magnitude (Hayes & Waldbauer, 2006; Sleep & Bird, 2006). We estimate $F_{M,NOW}$ by combining the two largest quantified fluxes of nonvolcanic lithospheric CH_4; global oceanic microseepage of 18–48 Tg CH_4 year^{-1} (Hornafius *et al.*, 1999), and mud volcanoes 6–13 Tg CH_4 year^{-1} (Milkov *et al.*, 2003; Milkov & Etiope, 2005), yielding an estimate of 2.8–7.6 Tmol O_2 equivalents year^{-1}. Catling & Claire (2005) independently estimated $F_{M,NOW}$ ~2.5 Tmol O_2 equivalents year^{-1} from the bulk composition of sedimentary rocks. For the sake of rough estimation, we adopt $F_{V,NOW} = 1.5$ Tmol year^{-1} and $F_{M,NOW} = 1.5$ Tmol year^{-1}, although we note that our estimate of $F_{V,NOW}$ may be too large, $F_{M,NOW}$ too small, and that all these numbers have broad uncertainties.

We examine the steady-state behaviour of the modern-day atmosphere by substituting hydrogen escape $F_{E,NOW} = 0$, and oxidative weathering $F_W = k_W[O_2]^\beta$ into equation 15, to yield:

$$[O_2]\big|_{modern} = \left(\frac{F_{B,NOW} - (F_{V,NOW} + F_{M,NOW})}{k_W}\right)^{\frac{1}{\beta}} \quad [Tmol] \quad (16)$$

where we define $k_w = 0.021$ Tmol$^{2/3}$ year^{-1} from equation 16 using the modern values of the parameters. We see that modern oxygen levels are set numerically by the imbalance between F_B and $(F_V + F_M)$, are modulated by oxidative weathering constants, and have no direct dependence on CH_4 levels.

Solving equation 13 for $[CH_4]$ in the modern limit (i.e. $F_E \to 0$) yields:

$$[CH_4]\big|_{modern} = \frac{\phi_{CH4}}{k_{eff}[O_2]} \quad [Tmol] \quad (17)$$

Equation 17 is analogous to equation 8 defining k_{eff}, which predicts 1.7 ppm CH_4 when the modern parameters cited in Section 3.2 are substituted. The direct applicability of equation 17 to the Phanerozoic is somewhat complicated given our choice of an atmospheric k_{eff} for the entire AOB reservoir, which effectively couples the redox state of the atmosphere to that of the ocean. Equation 17 exhibits constant behaviour of ~18 000 Tmol CH_4 (~10^{-4} bar) above oxygen concentrations of ~1.8×10^5 Tmol O_2 (10^{-3} bars) for $\phi_{CH4} = 400$ Tmol year^{-1}, given the functional dependence of k_{eff} as described in Section 3.2 and shown in Fig. 3. These predicted levels of O_2 and CH_4 (10^{-3} and 10^{-4} bar, respectively) are perhaps relevant to the Mesoproterozoic, given that this estimate effectively releases the total flux of seafloor methane directly into an oxic atmosphere, a physical condition more likely to have occurred in a stratified Mesoproterozoic ocean (Anbar & Knoll, 2002).

During the Archean, we assume that oxygen concentrations were low and hence the oxidative weathering flux (F_W) was

negligible, as witnessed by the redox state of detrital minerals and the absence of continental redbeds (Holland, 1984; pp. 277–332).

Substituting the definition of the escape flux F_E (equation 12) and $F_W = 0$ into equation 15 we find that:

$$[CH_4]\big|_{Archean} = \frac{(F_V + F_M) - F_B}{k_{esc}} \quad [\text{Tmol}] \qquad (18)$$

From comparison with equation 16 we see that in the steady-state ancient and modern limits, oxygen and methane have opposite approximately constant behaviour dictated by the numerical values of the fluxes of organic carbon burial, volcanism, and metamorphism, and are both independent of the level of the trace redox gas. We refine the estimate in equation 18 by rearranging algebraically, and substitute the numeric value of k_{esc} converted from Tmol to bars using equation 11:

$$[CH_4]\big|_{Archean} = 1.5 \times 10^{-4} \left(F_{V,NOW}\frac{F_V}{F_{V,NOW}} + F_{M,NOW}\frac{F_M}{F_{M,NOW}} - F_{B,NOW}\frac{F_B}{F_{B,NOW}} \right) \quad [\text{bars}] \qquad (19)$$

If we make the first-order assumption that F_B has remained constant over Earth history (i.e. $F_B = F_{B,NOW}$), we can derive a rough estimate for the CH_4 content of the Archean atmosphere. Making this assumption and substituting the given numeric values for $F_{V,NOW}$, $F_{B,NOW}$ and $F_{M,NOW}$, we find:

$$[CH_4]\big|_{Archean} = 1.5 \times 10^{-3}\,\text{bar} \times \left(\frac{3}{20}\left(\frac{F_M}{F_{M,NOW}} + \frac{F_V}{F_{V,NOW}} \right) - 1 \right) \qquad (20)$$

an estimate applicable only if the combined Archean volcanic and metamorphic reductant fluxes are ~7 times higher than modern values, agreeing with our earlier theoretical conclusion that enhanced reductant fluxes are required in order to maintain an anoxic atmosphere. If, as we argue is theoretically possible in Section 5.1, F_M may have reached 20 times its current value, equation 20 predicts steady state CH_4 partial pressures of 0.003 bar or 3000 ppmv, even in the absence of mantle redox evolution. This simple analytic estimate agrees surprisingly well with the results of sophisticated photochemical models of the Archean atmosphere (Zahnle, 1986; Kasting & Brown, 1998). In addition, equation 20 predicts that CH_4 concentrations will decrease with decreasing $F_M + F_V$ which is compatible with the notion that the left-hand side of equation 13 will be negative as long as F_E is large (i.e. throughout the Archean), so we expect CH_4 concentrations should consistently drop in quasi-steady state through the Archean.

An analytic estimate for Archean oxygen levels is obtained by solving equations 13 and 14 in steady state and eliminating $k_{esc}[CH_4]$ to obtain an alternate steady state solution:

$$0 = \phi_{CH4} - k_{eff}[O_2][CH_4] + F_B - (F_V + F_M + F_W) \qquad (21)$$

To obtain an estimate for Archean oxygen levels, we take $F_W = 0$ and solve equation 21 for $[O_2]$ to find:

$$[O_2]\big|_{Archean} = \frac{\phi_{CH4} + F_B - (F_V + F_M)}{k_{eff}[CH_4]} \quad [\text{Tmol}] \qquad (22)$$

Assuming $\phi_{CH4} \gg F_B - (F_V + F_M)$, taking a representative low oxygen/high methane k_{eff} value of 10^{-3} from Fig. 3, using $\phi_{CH4} = 400$ Tmol year^{-1}, and converting from Tmol to bar we estimate:

$$[O_2]\big|_{Archean} \cong \frac{1.2 \times 10^{-11}}{CH_4(\text{bar})} \quad [\text{bar}] \qquad (23)$$

Using the estimate of Archean CH_4 derived above (0.003 bar), equation 23 predicts a steady state Archean O_2 value of 4×10^{-9} bar. This simple analytical estimate, which neglects complications such as horizontal and vertical variations, is consistent with results from detailed photochemical models (Pavlov *et al.*, 2001).

The analytic solutions of our proposed equations 13 and 14 in the limits of low and high O_2 values support the general theoretical expectations of how the redox state of the atmosphere should evolve, as discussed in Section 2. In general, our analytic results show that either O_2 or CH_4 will control the redox state of the atmosphere. The amount of the dominant gas in both limits (equations 16 and 18) is strongly influenced by the quantity $F_B - (F_V + F_M)$, while the trace redox gas (equations 17 and 22) are strong reciprocal functions of the dominant gas. The nonlinearity of k_{eff} and F_W precludes simple analytic solutions in the transitional regime, and necessitates a numerical solution.

4.1 A definition for the oxic transition: K_{OXY}, the oxygenation parameter

An anoxic atmosphere can be defined as an atmosphere with an excess of H-bearing gases, such as H_2 and CH_4. Our modern atmosphere is called oxic given that the source of these reducing gases (volcanism, metamorphism) has been overwhelmed by the flux of oxidizing gases from the biosphere. On the ancient Earth, however, the proportions of reductants emanating from the planet were likely larger, and would have overwhelmed the oxygen source, forcing the atmosphere to be anoxic.

To make the above statements quantitative, we follow the approach described in Catling & Claire (2005) and motivated by the analytical results above, define an oxygenation parameter, K_{OXY}, based on the proportion of kinetically active gases in the ground-level atmosphere:

$$K_{OXY} = \frac{F_{SOURCE}}{F_{REDUCED\ SINKS}} \sim \frac{F_B}{F_V + F_M} \qquad (24)$$

If $K_{OXY} > 1$, the source of free oxygen outweighs the sinks and the atmosphere is oxic. The modern atmosphere has K_{OXY}

of 3 when one considers, as we do in this paper, only the carbon cycle as contributing to F_B. If the sulfur cycle is included (which is necessary for a quantitatively significant exploration of the Proterozoic and Phanerozoic (Holland, 2002)), the modern value of K_{OXY} is ~6 (Catling & Claire, 2005). In our numerical results, we define the 'oxic transition' as the first timestep at which $K_{OXY} > 1$.

5. NUMERICAL APPROACH

We now define first-order parameterizations of various Earth system fluxes. The parameterizations and constants used for our model are summarized in Table 1. Extensions to some of these parameterizations are described in Section 7.1.

5.1 Discussion of parameterizations

Reservoirs and redox fluxes in the box model are shown as Fig. 2. The atmosphere and dissolved gases in the upper ocean equilibrate on timescales of $10–10^3$ years (Berner, 2004; pp. 3–5). Therefore, we do not resolve changes to the atmosphere/ocean/biosphere AOB reservoir that occur on shorter timescales. Our choice of a coupled AOB reservoir also precludes us from testing hypothetical ideas regarding the Proterozoic in which the surface and deep ocean existed in separate redox states (Canfield, 1998; Anbar & Knoll, 2002; Huston & Logan, 2004), so we limit ourselves to considering the Palaeoproterozoic oxic transition only. The parameterizations that have been described previously are presented in the upper section of Table 1. Parameterizations for the evolution of the continental redox state and metamorphic degassing have not been previously been described in the literature. We develop first-order parameterization for these processes below and summarize them in the lower portion of Table 1.

5.1.1 The crust

We define the boundary between our upper and lower crust by the hydrological horizon below which weathering becomes largely unimportant, as opposed to more traditional definition based on the seismic velocity discontinuity at ~15 km. The pore depth (and hence the weathering depth) of the crust is ~5 km (Manning & Ingebritsen, 1999) while the average thickness is ~41 km (Rudnick *et al.*, 1998). By our definition, the upper crust comprises ~5/41 the mass of the total continental crust (2×10^{25} g), so we take our upper crust to be 2.44×10^{24} g and our lower crust as 1.75×10^{25} g, assuming, for simplicity, a constant mean density.

We are primarily concerned with modelling the 'hard rocks' (igneous and high-grade metamorphic) of the continental crust that contain excess ferric iron when compared to mid-ocean ridge basalts (Sleep, 2005a). These rocks are generally older than 2 Gyr in age (Patchett & Arndt, 1986; Sleep, 2005b). These hard rocks need to be considered separately from 'soft' continental rocks, which are sedimentary rocks. Data regarding the redox evolution of shales and other soft rocks were conceptually incorporated into our parameterization of F_W, but indicators from sedimentary environments (red beds, palaeosols, etc.) do not directly help us in quantifying the redox evolution of hard rocks. Our model primarily applies to the late Archean after the evolution of oxygenic photosynthesis, a time period at which most continent growth scenarios have reached the present-day area. For simplicity, we chose not to model continental growth, implicitly assuming a steady-state volume for the continental crust. This simplification is justifiable as the crustal fluid parameterization we develop depends on the redox state of the crust rather than the absolute amount of the crust. Carbon isotopes constrain the oxygen (organic burial) flux only relative to the input flux of CO_2, so the relative sizes of fluxes matter not their absolute amount.

The weight percentage of iron in the continental crust is ~7% (Taylor & McLennan, 1995), which is similar to the mantle value of 6.26 weight percentage (McDonough & Sun, 1995). Currently the amount of iron is not equivalent in the upper and lower crust (less total iron in upper crust than in lower crust), but there is no a priori reason to believe the crust would have formed in this fashion. For simplicity, we assume that 7% of the mass in both initial reservoirs is iron. Ultimately, all components of the crust must have been formed from mantle-derived igneous rocks. Thus, the reference percentage of Fe^{3+} from which we define 'excess' Fe^{3+} in the crust is best taken from fresh mantle-derived igneous rock, for which mid-ocean ridge basalt (MORB) is a good standard. As an estimate for the initial portioning between ferrous and ferric iron, we take Fe^{3+}/Fe^{2+} ratio of 0.111 from measurements of fresh MORB which cluster near a common value of 10% ferric and 90% ferrous (Bezos & Humler, 2005). For comparison, the ferric to ferrous ratio in the modern crust is ~0.25 as estimated from modern continental basalts ($Fe^{3+}/Fe^{2+} = 0.223$) (Holland, 1984; pp. 52–53) and from Mesozoic granites as $Fe^{3+}/Fe^{2+} = 0.25$ (Silver & Chappell, 1988; Kemp & Hawkesworth, 2004).

Reductants in the crustal boxes are tracked as Fe^{2+} directly and Fe^{3+} indirectly, fixed by assuming that $Fe_{total} = Fe^{2+} + Fe^{3+}$ remains constant in the absence of significant quantities of native Fe^0. Organic carbon (C^0) is also tracked. In this simplified model, once carbon enters the crust, it is converted to Fe^{2+} equivalents. A justification for this simplification is that ferric iron is easily reduced by graphite in metamorphism (e.g. $6Fe_2O_3 + C = 4Fe_3O_4 + CO_2$ in greenschist facies (Melnik, 1982; p. 182)). Two processes change the ferrous/ferric ratio in the crustal reservoirs: the reductant fluxes described in Sections 2 and 3, and geological mixing of the crust via weathering and tectonics. The reductants are tracked as mass concentrations (mass Fe^{2+}/total Fe mass), in variables [U] in the upper crust and [L] in the lower crust. We use mixing times τ_U and τ_L for the upper and lower crust, respectively. Using the average chemical sedimentary load of $\sim 4 \times 10^{15}$ g year^{-1} (Garrels & Mackenzie, 1971; p. 120) allows us to estimate τ_U

Table 1 Parameterizations in the model. On the following page are the 'enhanced' parameterizations described in section 7. The following parameterizations are given in the text and not reproduced here: k_{eff} is shown as Fig. 3. Crustal mixing is shown as equation 25, $\Delta fO_2(Fe^{2+}/Fe^{3+})$ is equation 27. Numerical values are in Tmol O_2 equivalents year^{-1} unless otherwise quoted

Symbol	Name	Parameterization	Discussion
Q	Heat flow	$(4.5/(4.5 - t))^{\eta}$	A dimensionless analytic approximation to heat flow models calculated from radioactive decay, where $\eta = 0.7$ (Sleep & Zahnle, 2001). Time t is in Ga from 4.5 to 0 at the present day.
F_B	Burial	$1/5 k_B(F_{CO2,V} + F_{CO2,M})$	We assume that the global O_2 flux due to organic carbon burial has remained approximately 1/5 of the total CO_2 outgassing rate over Earth history since oxygenic photosynthesis appeared, given the approximate constancy of organic carbon and carbon isotope fractionation in sedimentary rocks. $F_{CO2,M}$ is defined in equation 29, and we take $F_{CO2,V} = F_{CO2,V,NOW} * Q$. We set $k_B = 10/6$ (unitless) by substituting $F_{B,NOW} = 10$ Tmol year^{-1} (Holland, 2002), $F_{CO2,V,NOW} = 10$ Tmol year^{-1}, and $F_{CO2,M,NOW} = 20$ Tmol year^{-1} (Morner & Etiope, 2002).
F_E	H escape	$k_{esc}[CH_4]$	Diffusion limited hydrogen escape is assumed to have acted over Earth history (Walker, 1977; pp. 157–163) $k_{esc} = 3.7 \times 10^{-5}$ Tmol O_2 equivalents year^{-1} (Tmol CH_4)$^{-1}$.
F_W	Oxidative weathering	$k_w[O_2]^{\beta}$	The functional form of oxidative weathering suggested by Walker (1977), pp.103–105. Oxidative weathering should be negligible if oxygen concentrations are low, it should be roughly proportional to oxygen levels at intermediate values, and relatively insensitive at high oxygen levels. We use $\beta = 0.4$ but acknowledge that this parameterization is uncertain, e.g. (Holland, 2003), so we investigate multiple values of β in the perturbation analysis. $k_w = 0.037$ Tmol$^{0.7}$ year^{-1}.
ϕ_{CH4}	Net biosphere	400 Tmol year^{-1}	An estimate of the preindustrial *gross* flux of CH_4 from the degradation of photosynthetic organic carbon by methanogens, assuming the absence of sulfate reducers (see Section 3.1).
$\chi_{H_2,CSAT}$	H_2/CO_2 ratio C^0–saturated metamorphic gases	a) $0.058e^{-1.75\Delta fO_2}$ b) $0.012e^{-2.44\Delta fO_2}$ c) $0.072e^{-0.85\Delta fO_2}$	Analytic fits to average ratio in Fig. 6(A). Curve (a) is used for the ΔfO_2 range of [–3.0,–2.2], curve (b) for [–2.2,–1.2], curve (c) for [–1.2,2.0]. A lonear combination of the respective fits was made to smoothly join the curves in the ranges ΔfO_2 = [–2.3,–2.1] and ΔfO_2 = [–1.3,–1.1].
$\chi_{CH_4,CSAT}$	CH_4/CO_2 ratio C^0–saturated metamorphic gases	a) $14.08e^{-1.23\Delta fO_2}$ b) $0.06e^{-5.02\Delta fO_2}$ c) $0.194e^{-1.36\Delta fO_2}$	Analytic fits to average ratio in Fig. 6(B). Curve (a) is used for the ΔfO_2 range of [–3.0,–1.4], curve (b) for [–1.4,–0.2], and curve (c) for [–0.2,2.0]. A linear combination of the respective fits was made to smoothly join the curves in the ranges ΔfO_2 = [–1.5,–1.3] and ΔfO_2 = [–0.4,0.0].
$\chi_{H_2,NONSAT}$	H_2/CO_2 ratio C^0-activity metamorphic gases	a) $0.383e^{-1.59\Delta fO_2}$ b) $0.025e^{-2.79\Delta fO_2}$ c) $0.187e^{-0.87\Delta fO_2}$	Analytic fits to hybrid curve in Fig. 6(C). Curve (a) is used for the ΔfO_2 range of [–3.0,–2.2], curve (b) for [–2.2,–1.2], and curve (c) for [–1.2,2.0]. A linear combination of the respective fits was made to smoothly join the curves in the ranges ΔfO_2 = [–2.3,–2.1] and ΔfO_2 = [–1.3,–1.1].
$\chi_{CH_4NONSAT}$	CH_4/CO_2 ratio low C^0 activity metamorphic gases	a) $1.323e^{-2.06\Delta fO_2}$ b) $0.015e^{-4.19\Delta fO_2}$ c) $0.263e^{-0.76\Delta fO_2}$	Analytic fits to hybrid curve in Fig. 6(D). Curve (a) is used for the ΔfO_2 range of [–3.0,–1.9], curve (b) for [–1.9,–0.8], and curve (c) for [–0.8,2.0]. A linear combination of the respective fits was made to smoothly join the curves in the ranges ΔfO_2 = [–2.0,–1.8] and ΔfO_2 = [–1.0,–0.7].
χ_{H_2}	H_2/CO_2 ratio metamorphic gases	$\frac{\chi_{H_2,CSAT} + \chi_{H_2,NONSAT}}{2}$	To first order, we assume equal contributions from metamorphism of graphite-saturated rocks and rocks with low graphite activity. Representative values include: $\chi_{H2}(QFM - 1) = 0.308$, $\chi_{H2}(QFM) = 0.1296$, and $\chi_{H2}(QFM + 1) = 0.054$.
χ_{CH_4}	CH_4/CO_2 ratio metamorphic gases	$\frac{\chi_{CH_4,CSAT} + \chi_{CH_4,NONSAT}}{2}$	To first order, we assume equal contributions from metamorphism of graphite-saturated rocks and rocks with low graphite activity. Representative values include: $\chi_{CH4}(QFM) = 5.053$, $\chi_{CH4}(QFM) = 0.2289$, and $\chi_{CH4}(QFM + 1) = 0.086$.
F_M	Metamorphic outgassing of reductants	$k_m Q\left[\frac{F_{C,NV,NOW}}{1 + \chi_{CH_4}}\left(\chi_{H_2} + \chi_{CH_4}\right)\right]$	Assuming the modern crust can be approximated by QFM allows us to calculate $k_m = 0.256$ (unitless) by setting $F_{M,NOW} = 1.5$ Tmol year^{-1}, $\chi_{H2,NOW} = 0.13$, $\chi_{CH4,NOW} = 0.23$, $Q_{NOW} = 1$, and $F_{C,TOTAL} = 20$ Tmol year^{-1}. Assuming the crust is buffered at QFM + 1 yields $k_m = 0.58$. We varied k_m to tune the reference model to transition near 2.4 Ga, and adopted a tuned value of $k_m = 0.34$ for the reference model calculations.
F_V	Volcanic flux of reductants	$k_V F_{CO2,V}$	We define $k_{V,NOW} = 0.15$ by setting $\chi_{H2,V,NOW} = 1$ and assuming $F_{V,NOW} = 1.5$ Tmol O_2-consuming equivalents year^{-1} and $F_{CO2,V,NOW} = 10$ Tmol year^{-1}. We account for the maximum allowable mantle redox evolution by multiplying $K_{V,NOW}$ by $Q^{1/2}$, a factor which drops by ~2 over the course of Earth history. The use of $K_V = K_{V,NOW}Q^{1/2}$ is solely a numerical convenience without physical in the heat flow, given that oxygen fugacity increases with temperature at pressure.

Table 1 *Continued*

Symbol	Name	Parameterization	Discussion
$T_{EFF}(t)$	Effective temperature of the Earth	$T_{EFF,NOW} \times (1/(1 + 0.0835 * t))^{0.25}$	t in Ga from 4.5 to the present at 0. $T_{EFF,NOW}$ = 255K using modern values of the solar constant with an albedo of 0.3.
a(T)	Ice-albedo effect	T < 273: a = 0.6, T < 276: a = –0.083T + 23.3	Parameterization of linear albedo increase between 3 °C and 0 °C.
GAT	Global average temperature	GAT = $T_{EFF}(t)$ + f([CH_4], [CO_2],a(T))	GAT was fixed at 288K in reference model. In the enhanced model, GAT was calculated from the temperature parameterizations of Caldeira & Kasting (1992a) and Kasting *et al*. (2001), with the ranges of applicability described in the text. The Kasting *et al*. (2001) model was specifically calculated for a solar constant of 2.8 Ga, so we compute the greenhouse effect as $f = T_{KASTING}(CH_4,CO_2) - T_{EFF}(2.8\ Ga)$, where $T_{EFF}(2.8\ Ga) \sim 242K$.
cyano(T)	Temperature-dependent growth curve	$\left[\mu_{MAX} - \mu_{MAX}\left(\frac{(T_{OPT} - T)}{\Delta T}\right)^2\right] \times EXP\left(-\frac{\lvert T - T_{OPT}\rvert^3}{T_{REF}}\right)$	μ_{MAX} = 0.75 (doublings per day), T_{OPT} = 28 °C, ΔT = 28 °C, T_{LOW} = 0 °C, T_{HIGH} = 46 °C, T_{REF} = 1400. The functional form is taken from (Tang *et al*., 1997). These parameters were chosen to match the composite data described in the caption for Fig. 12(B). cyano(T) formally has units of μ (doublings per day), although we use it in ϕ_{CH4_NEW} as a dimensionless quantity. The 'Lovelock' parameterization is parabolic: μ_{MAX} = 0.38, T_{OPT} = 9 °C, ΔT = 18 °C, without an exponential cutoff.
ϕ_{CH4_NEW}	Temperature-dependent biosphere	ψ × cyano(GAT-273)	The maximum value of cyano(T) is 0.75 at T = 28 °C, so ψ = 680 Tmol $year^{-1}$ ensures that $\phi_{CH4} = \phi_{CH4\_NEW}$(15 °C) = 400 Tmol $year^{-1}$ to be compatible with the reference model. Similarly, ψ = 1273 Tmol $year^{-1}$ ensures that the 'Lovelock' parameterization is compatible with the reference model.

~200–500 Myr (we adopt $\tau_U \approx 400$ Myr) as the time to weather the upper crust and $\tau_L \sim 4$ Gyr for the lower crust. We implement crustal evolution using these time constants as follows:

$$\begin{aligned}\frac{d}{dt}[U] &= \frac{1}{\tau_U}([L] - [U]) + 4 \times (F_B - F_W)\\ \frac{d}{dt}[L] &= \frac{1}{\tau_L}([U] - [L]) - 4 \times F_M\end{aligned} \tag{25}$$

Here, the factors of 4 arise because we track all our fluxes in equivalent moles of O_2 that are consumed or produced, i.e. 4 mol of Fe^{2+} are oxidized to Fe^{3+} by 1 mol of O_2 via:

$$4FeO + O_2 \rightarrow 2Fe_2O_3 \tag{26}$$

Thus, in equation 25, a mole of O_2 contributed by the flux of organic burial (F_B) would add a reduced carbon or equivalently 4 mol of ferrous iron to the upper crust. Similarly, reductants released from the lower crust in the metamorphic reduced flux (F_M) sufficient to consume a mole of O_2 in the AOB system would remove 4 mol of equivalent ferrous iron from the lower crust (in reactions such as $H_2O + 2FeO = Fe_2O_3 + H_2$).

5.1.2 Redox evolution of the crust and metamorphic gases

Metamorphism is often considered redox neutral given that typical reactions such as graphite + $2H_2O \rightarrow CO_2 + 2H_2$ provide zero net redox change. However, when some of the resulting hydrogen irreversibly escapes the Earth, the net crustal reaction becomes an effective oxidation of graphite to limestone/marble. Any future metamorphic processing of the resultant crust must release slightly less reducing fluids by redox balance because the crust is now slightly more oxidized. The global reservoir of combined CO_2 is large, so this process would be unlikely to dramatically shift the $\delta^{13}C$ of the crust. We specify the redox evolution of metamorphic gases in a two-step manner. At each timestep, we calculate the oxygen fugacity of the lower crust, and then use that oxygen fugacity to calculate the composition of gases emanating from a C-O-H equilibrium fluid at metamorphic temperatures and pressures.

5.1.2a Specification of oxygen fugacity

The complex redox geochemistry of the crust and mantle are often approximated by their similarity to laboratory buffers in pure-phase minerals. The oxygen fugacity is defined as the thermodynamic activity of oxygen in equilibrium with the rock suite (Frost, 1991), and its value is a function of temperature and pressure. We estimate the oxygen fugacity of the crust from high temperature silicate melt experiments that were extrapolated to subsolidus temperatures (Sack *et al*., 1980). This particular form of the parameterization, which we reproduce as equation 27, was recently re-validated for low temperatures and pressures via modern Mössbauer techniques (Partzsch *et al*., 2004).

$$\begin{aligned}f_{O_2} &= EXP\left(\left(Log\left(\frac{Fe^{3+}}{Fe^{2+}}\right) - b/T - c - \Sigma\right)/a\right)\\ \text{where}\quad \sum &= \sum_i d_i X_i\end{aligned} \tag{27}$$

We take a, b, c and d_i from the experimental data in Table 3 of Sack *et al*. (1980). The summation in equation 27 is taken over the main components of the crust ($X_i = SiO_2$, Al_2O_3, FeO, MgO, CaO, Na_2O, and K_2O), where the X_i are the bulk

compositions in weight percentage, which we take from values representative of the bulk continental crust (Rudnick & Gao, 2004). While the above parameterization is more directly applicable to the basaltic portions of the continental crust, we adopt it as a representative first-order parameterization for the entire crust, as it encompasses the general direction and magnitude of change recorded in known crustal oxybarometers (Donohue & Essene, 2000).

At a MORB-like Fe^{3+}/Fe^{2+} ratio of $0.1/0.9 = 0.111$, equation 27 predicts $\log(fO_2)$ of -15.8. At Fe^{3+}/Fe^{2+} of 0.25, equation 27 predicts $\log(fO_2)$ of -14.2, implying that the bulk crust might evolve ~1.5 log units in fO_2 from its initial to present configuration.

5.1.2b Redox state of metamorphic gases

At a given pressure P, temperature T, and oxygen fugacity fO_2, the equilibrium redox speciation of the most important gaseous fluids in the crust (i.e. H_2O, CO_2, CH_4, CO, H_2, O_2) is completely specified (Huizenga, 2001). We used the 'species' program from the Perple_X modelling package (Connolly, 1990; Connolly & Cesare, 1993) to calculate the C-O-H fluid speciation under a variety of P, T, and fO_2 conditions encountered during metamorphism. We use the hybrid Redlich–Kwong equation of state to calculate the C-O-H fluid speciation as a function of oxygen fugacity in a graphite saturated field, given that average sedimentary rocks show carbonate/reduced carbon ratios of ~4 : 1 and that uplifted metamorphic rocks contain 2–7% carbon by weight (Wedepohl, 1995). Not all metamorphosed rocks contain graphite, so we also computed a similar series of models with a graphite activity of 0.1.

Figure 4 illustrates typical Perple_X outputs, displaying the species fractionation of volatiles vs. oxygen fugacity at a pressure of 2 kbar and temperature of 500 °C for both the graphite saturated and the low graphite case. These conditions are typical of high thermal gradient metamorphism in the amphibolite field (Rogers & Santosh, 2004; p. 196). The oxygen fugacities are displayed relative to the quartz-fayalite-magnetite (QFM) buffer calculated by the following equation:

$$\log(\mathrm{QFM}) = 9.0 + 0.09(P-1)/T - 25738/T \quad (28)$$

where P is the pressure in atmospheres and T is the temperature in Kelvin (Ohmoto & Kerrick, 1977). If the crustal region represented by Fig. 4 drifted one log unit below QFM in fugacity space, the H_2/CO_2 ratio changes from ~0.001 to ~0.1, while the CH_4/CO_2 ratio changes from 0.13 to 14.3. This implies that while CO_2 is the dominant metamorphic gas today, metamorphosing a more reduced Archean crust may have produced very much more CH_4 and H_2 relative to CO_2.

To further explore this hypothesis, we constructed a grid of temperature and pressure ranging from 200 °C to 800 °C (in 100 °C increments) and from 2 kbar to 8 kbar (in 2 kbar increments, corresponding to depths of ~5–35 km) Fluid speciation was calculated for each of these (P/T) grid points for a variety of oxygen fugacities, allowing specification of the H_2/CO_2 and $(CH_4 + CO)/CO_2$ (hereafter referred to as CH_4/CO_2) ratios as function of P,T, and ΔfO_2, where ΔfO_2 is the oxygen fugacity relative to QFM for the given P/T conditions as specified by equation 28.

We calculate speciation ratios of $\chi_{H2} = H_2/CO_2$ and $\chi_{CH4} = CH_4/CO_2$ for low thermal gradients associated with subduction of oceanic lithosphere, medium thermal gradients associated with continental collisions, and high thermal gradients associated with regional and contact metamorphism (Rogers & Santosh, 2004; p. 196). Figure 5 plots χ_{H2} and χ_{CH4} vs. ΔfO_2 for each of the three standard metamorphic thermal gradients through our P/T grid, with an average result computed via a logarithmic mean at each ΔfO_2 value taken to be representative for each thermal gradient.

A complete solution to the problem of metamorphic gas fluxes would entail quantification of the relative importance of each of these three forms of metamorphism throughout Earth history, along with a specification of the evolution in bulk composition of metamorphosed rocks. Here, we make the first-order assumption that the proportions of metamorphic rock types in the available geological record serve as proxy for the relative proportions of thermal gradients encountered. Wedepohl (1995) compiled average compositions of both Archean and modern continental crust, and estimated the vertically averaged rock types of various metamorphic grades as 6.3 km of low- and medium-grade metamorphic rocks (gneiss, schist, amphibolite, and marble) and 19.1 km of high-grade metamorphic rocks (sum of felsic and mafic granulites). We therefore take 6.3/25.4–25% of metamorphism to occur under low- and medium-grade conditions (assumed equally distributed) and 75% of total metamorphism to occur under high-grade

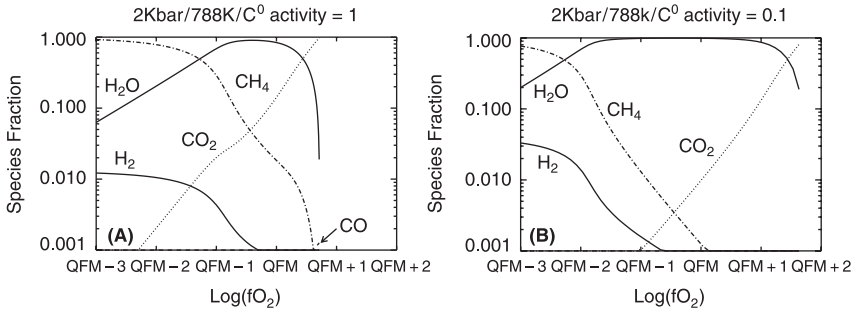

Fig. 4 Species fraction vs. oxygen fugacity for a rock suite at 2000 bar and 500 °C. (A) Calculation was performed using the hybrid Redlich–Kwong equation of state (equation 8 of the Perple_X's *species* package) for a carbon-oxygen-hydrogen fluid equilibrated within a graphite saturated field. (B) Calculation performed under same conditions but with graphite activity reduced to 0.1.

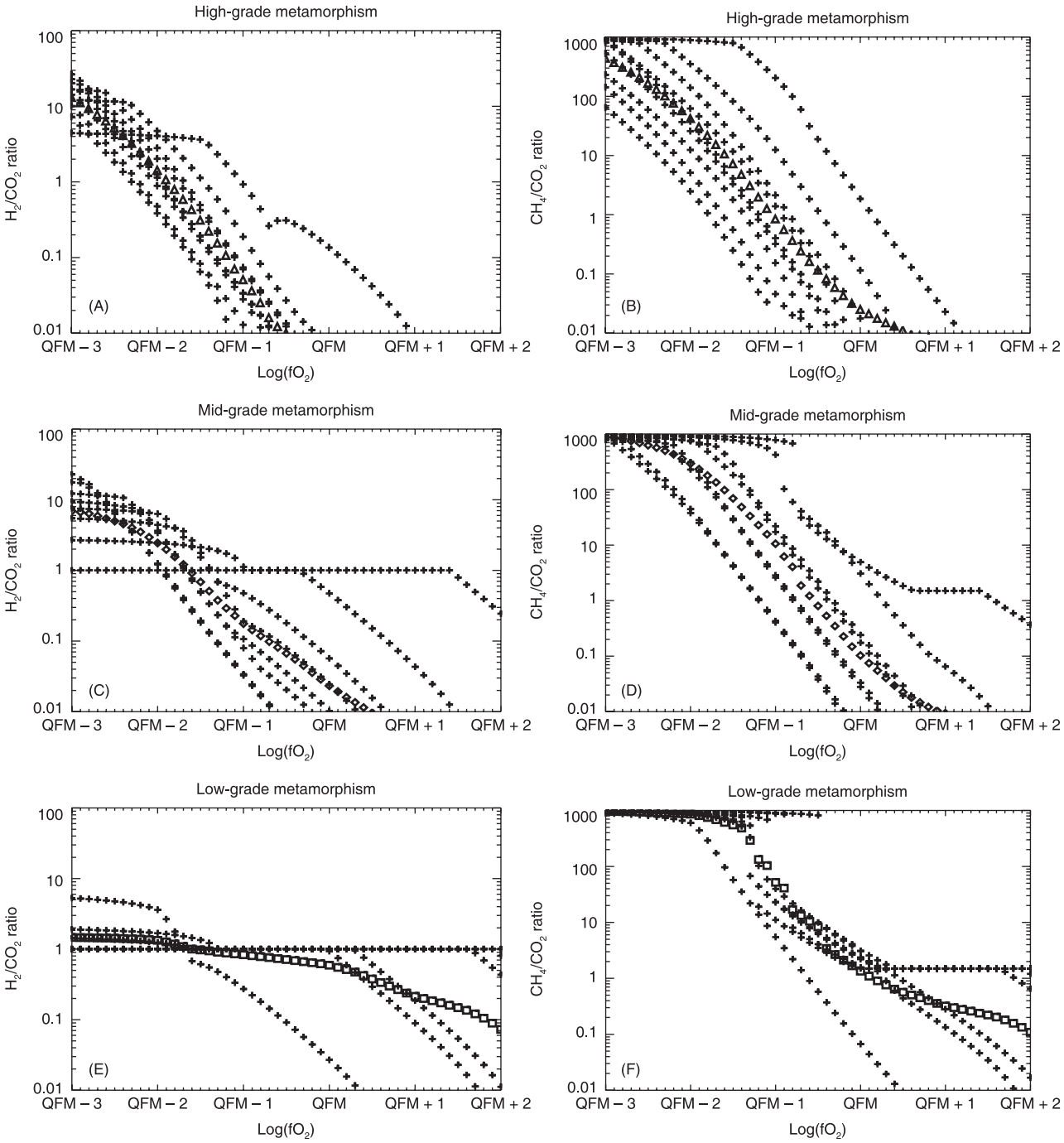

Fig. 5. Compilations of the graphite saturated H_2/CO_2 and CH_4/CO_2 ratios under various metamorphic conditions as a function of oxygen fugacity. Similar compilations were made for the low graphite activity case, but are not displayed. 5A–B) H_2/CO_2 and CH_4/CO_2 ratios for the following [P,T] grid of conditions encountered in high-grade metamorphism, in units of kilobars and °C: ([2,400], [2,500], [2,600], [2,700], [2,800], [4,600], [4,700], [4, 800], [6,700]). 5C–D) H_2/CO_2 and CH_4/CO_2 ratios for the following [P,T] conditions encountered in medium-grade metamorphism ([4,300], [4,400], [4,500], [6,500], [6,600], [6,700], [8,600], [8,700]). 5E–F) H_2/CO_2 and CH_4/CO_2 ratios for the following [P,T] grid of conditions encountered in low-grade metamorphism ([4,200], [6,200], [6,300], [6,400], [8,300], [8,400], [8,500]). Inferred conditions were taken from Fig. B3 in Appendix B of (Rogers & Santosh, 2004; p. 196). In each [P,T] pair, the oxygen fugacity was normalized to QFM via Equation 28. The bold symbols on each plot (medium grade – diamonds, low grade – squares, high grade – triangles) are a weighted logarithmic mean of all the points. These means are redisplayed on Fig. 6.

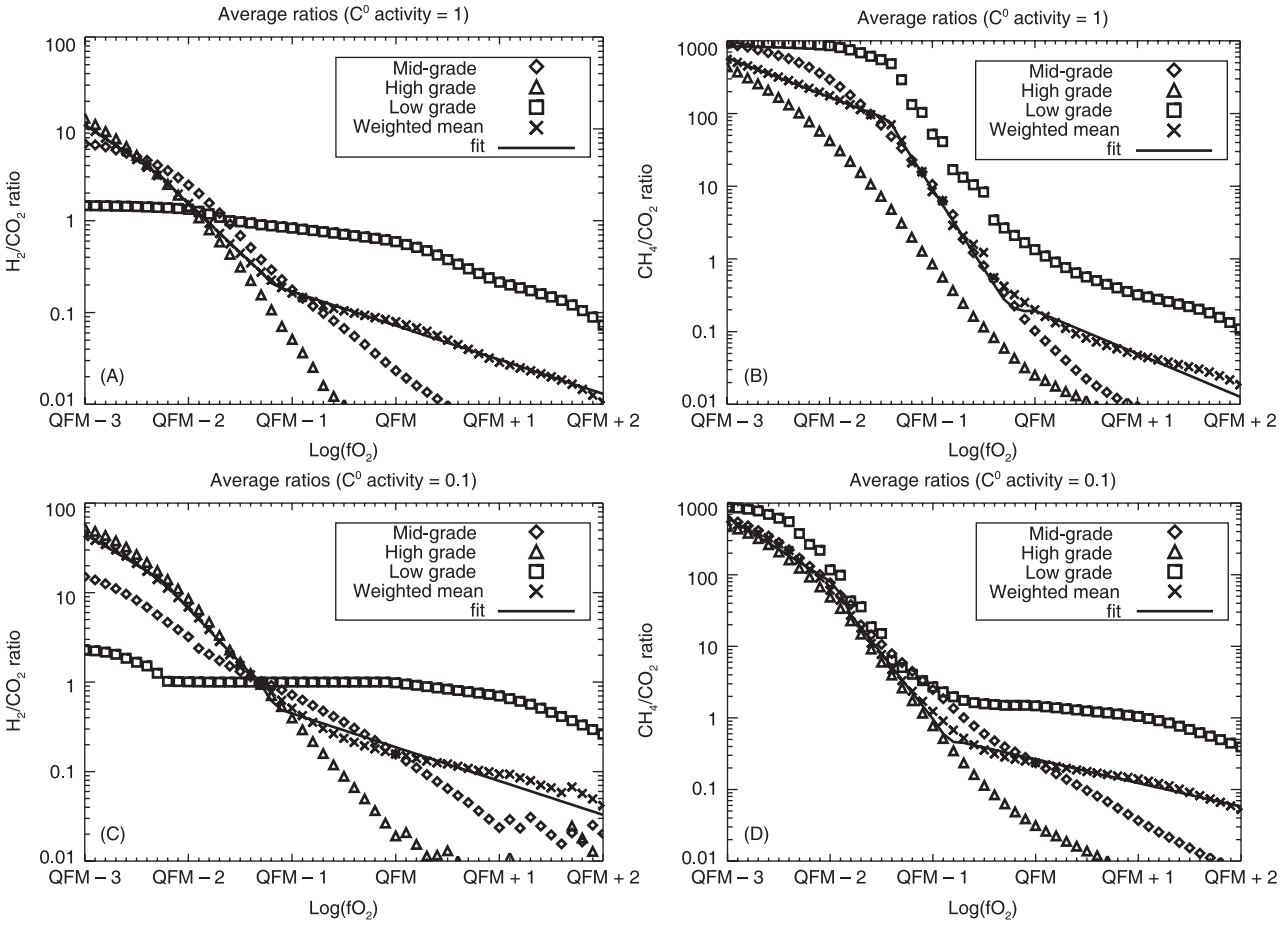

Fig. 6 Compilation of the average results displayed in Fig. 5. A weighted linear mean (crosses) at each ΔfO_2 was calculated by assuming 75% high-grade metamorphism (triangles), 12.5% medium-grade metamorphism (diamonds), and 12.5% low-grade metamorphism (squares). Analytic fits to the data are shown as a solid line and are quantified in Table 1. (A, C) shows χH_2 (= H_2/CO_2) ratio for the graphite saturated and low graphite activity case, respectively, while 6B and 6D show χCH_4 (= CH_4/CO_2) ratio for the graphite saturated and low graphite activity case.

conditions. In Fig. 6, we compile the average results from each metamorphic gradient, and weight them by the above proportions. Analytic fits to these results are used in the numerical model and are presented in Table 1.

We have shown in Fig. 6 how the speciation ratios $\chi_{H2} = H_2/CO_2$ and $\chi_{CH4} = CH_4/CO_2$ of crustal metamorphic fluids vary as a function of oxygen fugacity. The final piece in our prescription of F_M is a description of the total flux of non-volcanic CO_2 through the crust ($F_{CO2,M}$) and how it may have evolved with time. Morner & Etiope (2002) estimate a 'conservative' lower limit for nonvolcanic total carbon degassing of $F_{C,NV,NOW}$ ~17 Tmol year^{-1}. We make the first-order assumption that the present measured levels of carbon degassing represent a steady-state flux of C-bearing fluids throughout the crust and adopt $F_{C,NV,NOW}$ = 20 Tmol year^{-1}. Overall planetary thermal gradients were higher in the past, as indicated by the absence of Archean blueschists, which are metamorphic rocks that form under conditions of low temperature and high pressure, and the rarity of Phanerozoic komatiites (Sleep & Windley, 1982; Christensen, 1985). We account for this in our model by multiplying F_{C,NV_NOW} by the heat flow parameter Q described in Table 1.

Fixing $F_{C,NV,NOW}$ as the total flux of C-bearing fluids allows us to define:

$$F_{CO_2,M} = Q\left[\frac{F_{C,NV,NOW}}{1+\chi_{CH_4}}\right] \text{ and } F_{CH_4,M} = Q\left[\frac{\chi_{CH_4}F_{C,NV,NOW}}{1+\chi_{CH_4}}\right] \quad (29)$$

which allows us to complete our description of F_M:

$$F_M = k_m(\chi_{H_2}F_{CO_2,M} + F_{CH_4,M}) = k_m Q\left[\frac{F_{C,NV,NOW}}{1+\chi_{CH_4}}(\chi_{H_2}+\chi_{CH_4})\right] \quad (30)$$

where k_m is a unitless constant that we use as a tuning parameter. End-member values for k_m of 0.25 and 0.6 are estimated in Table 1. We briefly note that radiolytic production of H_2 from H_2O might promote non-negligible crustal CH_4 fluxes from the Precambrian shield (Onstott *et al.*, 2006).

This process would oxidize the crust while adding additional reductants to the F_M flux.

5.2 Numerical code

The equations are solved via the reverse-Euler method with variable timesteps selected to ensure that the (discarded) nonlinear terms would have contributed less than 1% of the computed solution (Walker, 1990a). At each step, time-dependent changes are made to the fluxes, allowing the solution to evolve as a succession of quasi-steady states. We compute solutions from 4.0 Ga to the present, but do not consider our parameterizations as representative prior to the end of the late heavy bombardment era at 3.8 Ga. The fluxes are driven to modern day values at time = 0, but the computed solutions after the oxic transition are not likely to be as accurate given that we do not incorporate the sulfur cycle. A similar model that considers the sulfur cycle will be necessary to model the evolution of redox state during the Proterozoic.

6. MODEL RESULTS

First, we describe results using our parameterization of F_M described in Section 5.1. We subsequently refer to these results as the reference model. A generic feature of any box model is tunable parameters. Choices of tunable parameters are generally restricted to quantities that are less constrained by available data, with the hope that exploring the available parameter space to arrive at a self-consistent result will help constrain the unknown quantity. Referring to the formulae in Table 1, we used the quantities η (the heat flow exponent), β (the oxidative weathering exponent), and k_m (the metamorphic proportionality factor), as our tunable parameters. We used $\eta = 0.6$, $\beta = 0.4$ and $k_m = 0.43$ to tune the oxic transition in the reference model to occur near the observed time of 2.4 Ga.

The main results of the reference model are illustrated in Fig. 7. Figure 7(A) shows the evolution of atmospheric CH_4 and O_2, plotted in bars vs. time in Ga. As expected from the theoretical arguments and analytical results in Sections 3 and 4, the numerical model predicts an early atmosphere dominated by reducing gases with O_2 as a trace gas, followed by a geologically rapid transition to an atmosphere with significant O_2 and lower CH_4. Figure 7(B) shows the computed fluxes that drive the solutions of equations 13 and 14 shown in Fig. 7(A). Hydrogen escape (F_E) was a quantitatively important redox flux early in the reference model, with integration under the F_E curve in Fig. 7(B) yielding ~4.8 billion Tmol of oxygen equivalents added to the AOB prior to the oxic transition. In this same time period, 96.2 billion Tmol of oxygen equivalents are released from the crust by metamorphic degassing, while 93.1 billion Tmol are added via organic carbon burial, yielding a net gain in the crustal system of 1.7 billion Tmol oxygen equivalents. The self-consistent computation of 1.7 billion Tmol of net oxidation in the crustal reservoir, although subject to large uncertainties, is consistent with the previously mentioned compilations of oxygen excess in 'hard' igneous and high-grade metamorphic crustal rocks (Catling *et al.*, 2001; Sleep, 2005a). Crustal oxidation slowly reduces the flux of reduced species in metamorphic gases, which in turn reduces the magnitude of reductants (F_M) from the metamorphosed crust, eventually driving $K_{OXY} > 1$ and a transition to an oxic atmosphere. By the time of the transition, hydrogen escape (F_E) is a minimal redox flux, given the drop in CH_4 levels. At this point, the steady-state CH_4 mixing ratio is set by the approximate balance between the ground level flux and atmospheric destruction (see equation 13 with $F_E \rightarrow (0)$ so that $\phi CH_4 \approx k_{eff}[O_2][CH_4]$ at the time of transition. In addition, oxidative weathering of the crust (F_W) has not yet become a significant redox term, so the quantitatively important fluxes at the time of the transition are F_B, F_V, and F_M. These fluxes are numerically much smaller than the gross flux of methane ϕCH_4, or its oxidation loss, but it is the difference between F_B and $F_V + F_M$ that appears to matter for the redox evolution of the atmosphere.

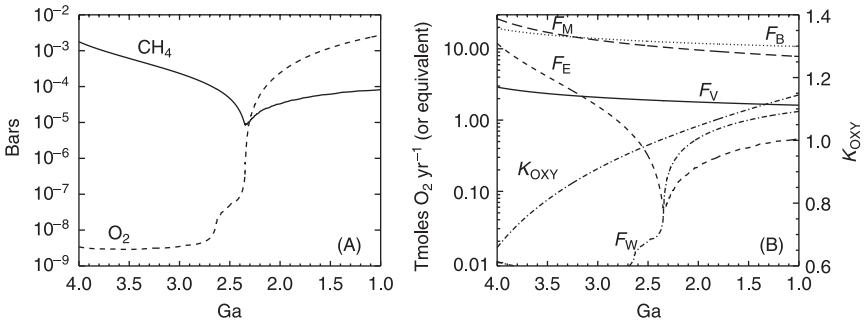

Fig. 7 (A) Evolution of atmospheric gases in the reference model. $[O_2]$ and $[CH_4]$ (in bars) are plotted vs. time (in Ga). Interpretation of bars as partial pressures requires the further assumption that Earth's atmospheric pressure has remained constant, which may or may not be the case depending on the nature of the ancient nitrogen cycle. The behaviour of the trace gas (i.e. O_2 prior to GOE and CH_4 after) is driven by the structure of $k_{eff}(O_2,CH_4)$ as shown in Fig. 3. (B) Evolution of Earth's major redox fluxes, shown on the logarithmic left-side axis in Tmol $year^{-1}$ normalized as O_2 equivalents. The right-side axis is a linear scale for the trace of K_{OXY}. In the reference model, K_{OXY} evolves from 0.7 at 3.8 Ga to 1.15 at 1 Ga, first becoming greater than 1 at $T_{OXY,RM} = 2.425$ Ga.

Restricting attention to the organic burial and outgassing reductant fluxes at the time of the oxic transition, condenses equation 14 for the evolution of atmospheric oxygen to:

$$\frac{d}{dt}[O_2]\Big|_{Trans} \sim F_B - (F_V + F_M) \qquad (31)$$

so the slight imbalance between the production of oxygen via organic carbon burial and the reducing gases from the solid planet is of critical importance. The atmosphere will transition from anoxic to oxic (i.e. from $K_{OXY} < 1$ to $K_{OXY} > 1$) when $F_V + F_M$ becomes quantitatively smaller than F_B. Assuming a constant F_B, the timing of the oxic transition is thus set by geological processes and the preceding history of enhanced hydrogen escape, which together regulate the decrease in reducing gases from volcanoes and metamorphism. The reference model is a numerically self-consistent example of this behaviour including both crustal redox evolution and limited mantle redox evolution as constrained by available data.

To further examine the issues surrounding the timing of the oxic transition, we performed a series of perturbations to the reference model. Our first experiment, shown as Fig. 8 consisted of numerically setting hydrogen escape (F_E) to 0. With this change, the reference model did not undergo an oxic transition, remaining in a Titan-like methane-rich atmosphere for over 4 Gyr, despite levels of oxygen input from organic burial similar to modern levels. This result provides numerical support to the earlier statement that there is no conflict between the coexistence of modern levels of oxygen production and an anoxic atmosphere. In this experiment, Earth is unable to permanently lose the reductants that emanate from the solid planet, so the planet as a whole does not evolve in redox state. Hydrogen escape is a physical process that acts on terrestrial planets, so we do not present Fig. 8 as being representative of a physically realistic Earth, but merely as a confirmation of the concept that hydrogen escape is vital to irreversibly oxidize a planet.

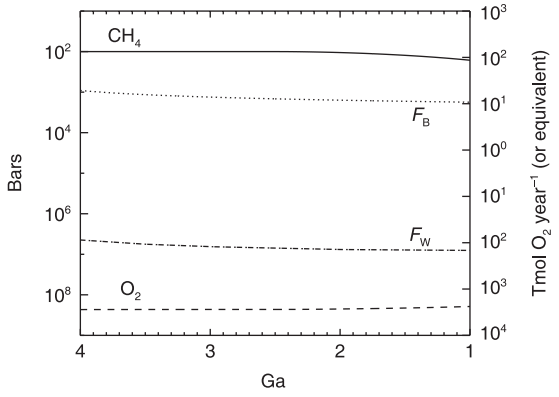

Fig. 8 An experiment with the reference model in which hydrogen escape, $F_E(t) = 0$. Atmospheric oxygen remains negligible despite a constant flux of organic carbon burial $F_B = 10$ Tmol year^{-1}, over Earth history. O_2 and CH_4 gases map to the left axis, while the F_B and F_W fluxes map to the right axis.

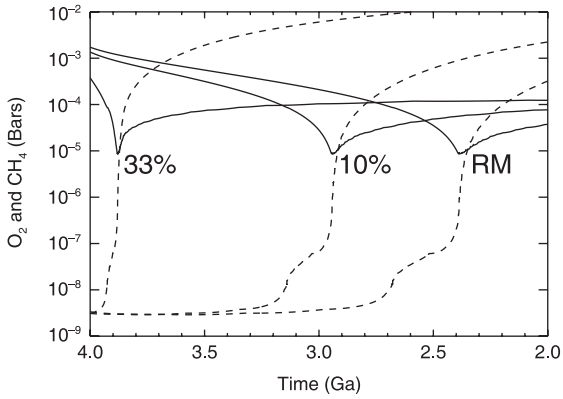

Fig. 9 Modelled traces of atmospheric composition of [CH_4] (solid lines) and [O_2] (dashed lines) in bars vs. time, as in Fig. 7(A). The right-most set of lines, marked by 'RM', are the [CH_4] and [O_2] curves from the reference model. The middle set of lines, marked by '10%', are the gas curves resulting from decreasing the numerical parameterization of F_M in the reference model by 10%. The left-most set of curves represents the gas curves that result from decreasing F_M by 33%.

We next examined the effect of decreasing the amount of reducing gases emanating from the crust. Our next experiment was to assume that metamorphic outgassing (F_M) was less important as a redox flux over Earth history. Figure 9 shows that reducing our numerical parameterization of F_M by decreasing k_m by 33% causes our reference model to transition within 10^8 years. This transition occurs when $F_B > F_E$ and the CH_4 concentration (and hence F_E) drops precipitously from its assumed initial condition without the influx of reductants from the solid planet. Figure 9 also shows an experiment in which F_M was decreased by 10% from the reference model values. In this experiment, we see that the amount of crustal degassing serves to significantly vary the timing of the oxic transition, and that quasi-steady state CH_4 levels increase with increasing F_M, as predicted by our analytical result in equation 20.

We next explored changes to k_{eff}, our parameterization of the effective destruction of CH_4 by O_2. Figure 10 shows that k_{eff} strongly affects the steady-state level of whichever gas is currently a trace gas (O_2 prior to the transition, CH_4 after), as well as the sharpness of the transition in time, but has no effect on the timing of the transition. The primary reason for this is that the appearance of atmospheric ozone is the driving factor in changing our atmospheric parameterization, and ozone does not begin to significantly appear in Earth's atmosphere until $O_2 > \sim 10^{-5}$ bar (Kasting, 1979). In the reference model, K_{OXY} first becomes larger than 1 at ~2.4 Ga, but the transition from O_2 to CH_4 dominated (by number) takes another 5 Myr. The crossover point occurs at ~2.35 Ga at which point $\sim 1 \times 10^{-5}$ bar of each gas exists in our model atmosphere. It is only after this crossover point that the effects of ozone production on CH_4 levels will become important. However, the exact speed of the transition in our reference model should not be taken as realistic since the model is merely an idealized

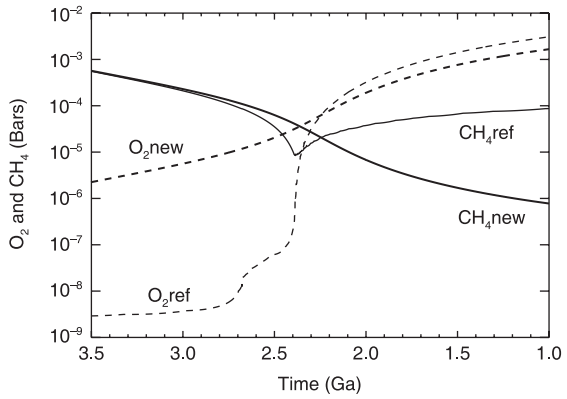

Fig. 10 The thick curves are atmospheric gas evolution curves (CH_4 = solid, O_2 = dashed) obtained from setting $k_{eff}(t) = 10^{-5}$ Tmol^{-1} year^{-1} in the reference model. For comparison, the reference model curves are plotted as thin curves. The effect on the timing of the transition and on the behaviour of the dominant redox gas is negligible. The behaviour of the trace redox gas is strongly affected by changes to k_{eff}.

redox representation and does not include feedbacks on the climate, biosphere or ocean chemistry (e.g. the increase in sulfate levels and diminution of methane fluxes to the atmosphere due to methanotrophy). In general, we expect the transition to be even more rapid than modelled.

After the oxic transition in our reference model, the k_{eff} parameterization allows CH_4 levels to re-ascend to ~100 ppm, which is compatible with other predictions of the Mesoproteoroic greenhouse (Pavlov *et al.*, 2003; Kasting, 2005). In addition, oxygen levels approach 1–10% PAL, consistent with other constraints on Proterozoic oxygen (Canfield *et al.*, 2000; Brocks *et al.*, 2005). That these results are obtained by attempting to drive the fluxes to modern day values raises the possibility that an additional buffer, likely sulfur, is needed to describe Proterozoic and Phanerozoic redox evolution. CH_4 rises in the Mesoproterozoic due to the complexities of atmospheric chemistry at intermediate oxygen levels. Ozone begins to form at oxygen levels of 10^{-5} bar, and rises nonlinearly with oxygen concentrations (Pavlov & Kasting, 2002). Ozone absorbs solar radiation between 200 and 320 nm, enhancing the CH_4 lifetime against photolytic destruction in the lower atmosphere, a process that competes with decreasing upper atmosphere CH_4 lifetimes due to the production of OH described in Section 3.2. These, and the net results of other complicated competing behaviours relating the methane lifetime, are captured within our para-meterization of k_{eff}. Equation 17 predicts that post-transition methane levels are proportional to $1/([O_2] \times k_{eff})$, and k_{eff} drops faster than O_2 rises in the pO_2 range between 10 and 1000 ppmv (Fig. 3), allowing for increasing CH_4 levels. Net methane fluxes may have decreased after the GOE due to greater respiration of organic matter using O_2 and sulfate, which would decrease the amount of methane predicted for the Proterozoic atmosphere.

Our results regarding the timing of the transition are limited to the statement that the timing of the transition depends on when $F_M + F_V$ drop below F_B in a permanent fashion. Curves similar to Fig. 7 can be obtained by decreasing parameterizations of F_V or even by increasing F_B while keeping F_M and F_V constant. As an example, Fig. 11 displays nearly identical results to Fig. 7, except that F_M was held approximately constant and F_V was arbitrarily made proportional to the square of the heat flow term, Q. Curves similar to Fig. 9 can be made by decreasing the total volcanic outgassing in a model similar to that of Fig. 11. In Section 2, we explained why the decreasing F_V scenario is difficult to reconcile with data on mantle oxygen fugacity or carbon isotopes, although models based on changing fluxes of hydrothermal cations (Holland, 2002; Kump & Seyfried, 2005) partially escape this criticism. The results shown in Fig. 11 are not internally self-consistent in that the crust becomes significantly reduced by organic carbon burial, although the simplicity of our model rules out further analysis on this issue. While not the only possible solution, we believe that the reference model discussed above (and shown in Fig. 7) forms the first numerically self-consistent model of Earth's redox fluxes that operates within all available constraints from the geological record. The model invokes large-scale changes in the proportions of reducing gases from the crust, a hypothesis that requires geochemical tests. The model predicts redox evolution within the hard rocks of the bulk Archean crust. The predictions of our reference model would be greatly bolstered when a stronger understanding of the both the modern and the ancient geothermal, hydrothermal, and metamorphic degassing history of the planet is obtained.

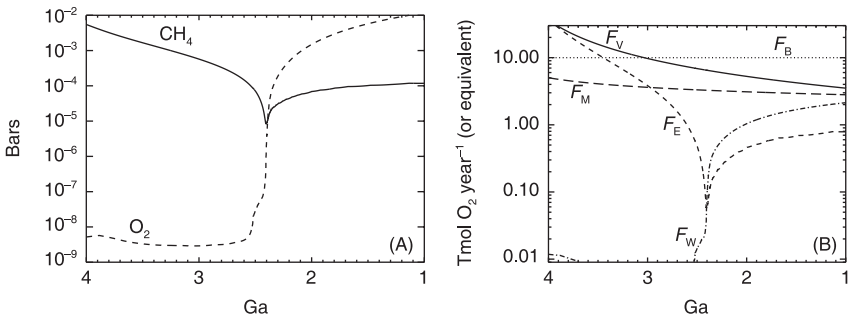

Fig. 11 (A) Evolution of atmospheric gases simulating a oxic transition driven by declining volcanic fluxes. [O_2] and [CH_4] (in bars) are plotted vs. time (in Ga). (B) Evolution of Earth's major redox fluxes which result in the gas curves shown in 11A, shown on the logarithmic left-side axis in Tmol year^{-1} normalized as O_2 equivalents.

Table 2 Results from a perturbative analysis of the reference model. In each case, a single variable (first column) was modified by a given factor (second column) and the perturbed reference model was run with only this change. The time of the oxic transition in the perturbed model ($T_{OXY,PERT}$) was computed from the first timestep when $K_{OXY} = 1$ in the perturbed model, and the normalized effect on the timing of the oxic transition is presented in the third column, with positive numbers reflecting an earlier oxic transition and negative numbers reflecting a later oxic transition

Variable	Factor	$(T_{OXY\_PERT}/T_{OXY\_REF}) - 1$
Initial $[CH_4]$	10x,	0.003
	1/10x	−0.009
Initial $[O_2]$	10x,	0.0
	1/10x	0.0
Initial iron in upper crust	5x	0.025
	2x	0.016
	1/2x	−0.035
	1/5x	−0.11
Initial iron in lower crust	5x	−0.743
	2x	−0.271
	1/2x	0.204
	1/5x	0.395
k_m	1/1.1	0.23
	1/1.3	0.509
	1/1.5	0.633
	1.1	−0.313
	1.2	−0.692
	1.3	no trans
β (F_W O_2 exp.)	2x	0
	1/2x	0
k_w	10x	0
	1/10x	0
η (heat flow exp.)	2x	−0.327
	1/2	0.438
k_{eff}	Many	0
F_E	1/10	−0.148
	1/100	−0.975

6.1 Sensitivity analysis – the timing of the oxic transition

In order to test the sensitivity of our model to its various parameters, we subjected the parameters of reference model to single perturbations, leaving all others unchanged. We compute the effect of the perturbation on the timing of the oxic transition by calculating the timestep in the perturbed model, $T_{OXY,PERT}$, at which K_{OXY} (defined by equation 24) first exceeds 1. We compare $T_{OXY,PERT}$ with $T_{OXY,RM} = 2.425$ Ga, which defines the time of the oxic transition in the reference model. Table 2 shows that the perturbations with the largest relative effects relate to the magnitude of metamorphic degassing, which is ultimately tied to the amount of iron in the continental crust. The largest relative perturbation we examined was that of reducing hydrogen escape (k_{esc}) in our reference model by two orders of magnitude, as recently suggested may have occurred (Tian *et al.*, 2005). This change prevents our model from transitioning until 0.06 Ga, an effect similar to increasing the amount of iron in the lower crust by a factor of 7. This result supports the general idea that Earth needs to lose reductants in order to oxidize, and shows that any model invoking slow hydrogen escape will likely require preferential subduction of reduced material to the mantle in order to conserve redox and explain an oxic transition at 2.4 Ga.

7. CLIMATE-BIOSPHERE FEEDBACKS

We purposefully created a reference model without many tuning parameters. We now discuss some first-order additions to some of the parameterizations, and their influence.

7.1 Climate feedbacks

Perhaps the most glaring omission in the reference model is a lack of surface temperature feedbacks. Methane is a strong greenhouse gas, and the collapse of this greenhouse gas upon the rise of O_2 would significantly affect temperature-dependent processes. Figure 1 of Pavlov *et al.* (2000) predicts that at a fixed CO_2 level in an anoxic atmosphere, a drop from 10^{-3} to 10^{-5} bar of CH_4 would decrease global average surface temperatures by 23K, a change that would likely affect the biosphere. The global temperature drop during the collapse of a methane greenhouse has been implicated in possible 'Snowball Earth' events (Pavlov *et al.*, 2000), which further impacts climate through the ice-albedo feedback.

We constructed a hybrid parameterization for the evolution of global average surface temperature based on atmospheric CH_4 and CO_2 levels from previously published radiative-convective modelling (Caldeira & Kasting, 1992a; Kasting *et al.*, 2001). The parameterizations of Kasting *et al.* (2001) are suitable for $10^{-5} < pCO_2 < 10^{-2}$ and $10^{-5} < pCH_4 < 10^{-2}$ in an anoxic atmosphere, whereas those of Caldeira & Kasting (1992a) are suitable for $10^{-8} < pCO_2 < 10^{-2}$ in an oxic atmosphere. We correct for solar luminosity evolution (Walter & Barry, 1991) keeping albedo fixed at 0.3 (although see below), and use the parameterization of Kasting *et al.* (2001) if $pCH_4 > 10^{-5}$, Caldeira and Kasting (1992a) if $pCH_4 < 10^{-6}$, with a logarithmic extrapolation at intermediate CH_4 levels. Our parameterization is suitable so long as we do not enter a regime in which $pCO_2 < 10^{-5}$ and $pCH_4 > 10^{-5}$. The temperature parameterization in the intermediate regime is presented as Fig. 12(A), for a solar luminosity at 2.4 Ga. The temperatures predicted by this parameterization at our computed CH_4 levels are supportive of a generally warm, but not hot, Archean climate (Sleep & Hessler, 2006). While this is a reasonable first-order parameterization, a full computation using a time-dependent radiative-convective model would be needed to verify the details through the intermediate oxic states (represented here by falling CH_4).

Our parameterization of the global average surface temperature drops below 0 °C for certain concentrations of CH_4 and CO_2, depending on the solar luminosity. If global ice cover exceeds a certain fraction, a runaway negative feedback might

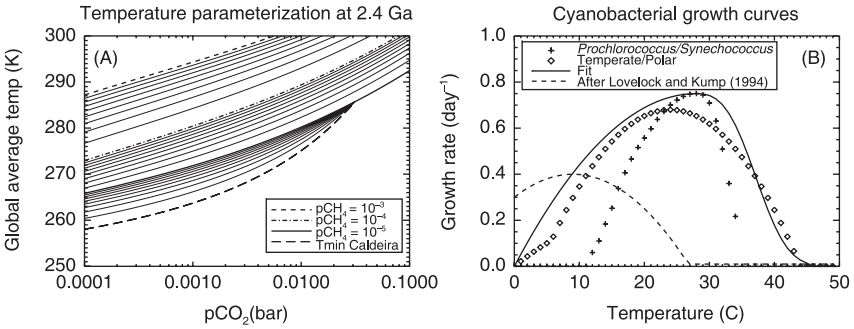

Fig. 12 Major parametric changes to the reference model. (A) A plot of our hybrid temperature parameterization. In the CH_4 range between concentrations of 10^{-6} and 10^{-5} we use a logarithmic weighted combination of the parameterizations of Kasting *et al*. (2001) and Caldeira & Kasting (1992a). Global average surface temperatures are shown for various concentrations of CH_4 and CO_2 computed for the solar constant at 2.4 Ga. The ice-albedo effect is not shown in this figure. (B) The temperature dependence of cyanobacterial growth. Growth rates, in doublings per day (μ), are plotted vs. temperature. Growth rate data for *Prochlorococcus marinus SS120* (μ_{MAX} = 0.63, T_{OPT} = 24 °C, ΔT = 11.5 °C, T_{LOW} = 12.5 °C, and T_{HIGH} = 28 °C) and *P. marinus MED4* (μ_{MAX} = 0.63, T_{OPT} = 24 °C, ΔT = 12 °C, T_{LOW} = 12 °C, and T_{HIGH} = 28 °C) from Moore *et al*. (1995) were averaged and combined those of *Synechococcus WH8103* (μ_{MAX} = 0.75, T_{OPT} = 28 °C, ΔT = 15.5 °C, T_{LOW} = 12.5 °C, and T_{HIGH} = 35 °C). An average of the 33 temperate cyanobacterial species from (Tang *et al*., 1997) were fit parabolically (i.e. using the form in Table 1 without the exponential cutoff) using μ_{MAX} = 0.68, T_{OPT} = 24 °C, ΔT = 20 °C. An average of the 27 polar cyanobacterial species from Tang *et al*. (1997) were fit parabolically using μ_{MAX} = 0.23, T_{OPT} = 20 °C, ΔT = 20 °C. A fit to the data is shown as a solid line, with coefficients given in Table 1. A composite cyanobacterial growth curve motivated by Lovelock & Kump (1994) is shown as a dashed line.

occur in which the increased reflectivity of ice (vs. land and ocean) accelerates the cooling of the planet. We modelled this 'ice-albedo' feedback with a linear increase in planetary albedo from 0.3 to 0.6 between global average temperatures of 3 °C and 0 °C, where we take the upper-limit value of 0.6 as a representative 'global average' albedo during a low-latitude glaciation event (Warren *et al*., 2002).

Escape from a 'Snowball Earth' at 2.4 Ga is a difficult proposition. The effective temperature of the Earth at 2.4 Ga is about −30 °C, so if the Earth was entirely frozen over due to a collapsing greenhouse, it follows that there needs to be a significant greenhouse in place upon thawing to keep the Earth system from re-freezing. One way of escaping a global glaciation is the volcanic build-up of CO_2 to levels approaching ~0.2 bar (Caldeira & Kasting, 1992b; Kirschvink, 1992), enhancing greenhouse warming to levels that melt the ice, with subsequent resumption of the carbonate-silicate cycle (Walker *et al*., 1981) leading to massive carbonate deposits and stabilization of the temperature (Hoffman & Schrag, 2002). To parameterize this, we implemented a simple 'carbon cycle' that attempts to maintain pCO_2 at 0.01 bar by balancing a constant CO_2 source with a sink proportional to $RCO_2^{0.5}$, where RCO_2 is the ratio of CO_2 to the modern level (Berner & Kothavala, 2001). When global average temperatures fall below 0 °C, the sink is turned off, allowing CO_2 levels to rise.

7.2 Biosphere–temperature feedbacks

We parameterize the temperature-dependent growth rates of cyanobacteria, the primary producers of our biosphere. Growth rates vary as a function of temperature for various genera of cyanobacteria that live at various latitudes. The maximum laboratory growth rates (generally reported in units of doublings per day with symbol μ) for many cyanobacteria occur around between 25 °C and 35 °C, with experimental data on temperature dependence usually fit by parabolas (Tang *et al*., 1997) and/or competing exponentials (Moisan *et al*., 2002). To create a general function for the temperature dependence of cyanobacterial activity, we combined growth rate data (Moore *et al*., 1995) for the two dominant species of cyanobacteria: *Prochlorococcus* and *Synechococcus*, with the data weighted 1 : 6.1 by their seasonally averaged abundance (DuRand *et al*., 2001). These species do not exhibit growth below 10–15 °C, so we assume globally colder temperatures would shift the global species balance towards the polar cyanobacteria, which are generally the dominant microbe in seasonal melt ponds on polar ice sheets (Tang *et al*., 1997). We add in the averaged growth rates of 24 polar cyanobacteria, combining these with the *Synechococcus/Prochlorococcus* data. Fitting an exponentially damped parabola to the combined data yields the curve shown in Fig. 12(B) and given parametrically as the unitless function cyano(T) in Table 1. Our cyanobacterial growth curve peaks at 28 °C, warmer than the current global average surface temperature of 15 °C that was assumed in the reference model. To account for this we modify our parameterization of ϕ_{CH4} to $\phi_{CH4\_NEW}(T) = 680$ Tmol year^{-1} × cyano(T), given that cyano(T_{max}) = 0.75. This formula was selected so that $\phi_{CH4} = \phi_{CH4\_NEW} = 400$ Tmol year^{-1} at 15 °C (as in the reference model), and has a new peak value of ϕ_{CH4_NEW} = 510 Tmol year^{-1} occurring at T_{max} = 28 °C.

Lovelock & Kump (1994) point out that nutrient availability potentially has a stronger effect on growth rates than temperature. Indeed, satellite observations of chlorophyll shows significantly greater chlorophyll abundance in polar regions compared to the tropics, likely due to enhanced ocean circulation in cooler water bringing ample nutrients from deeper

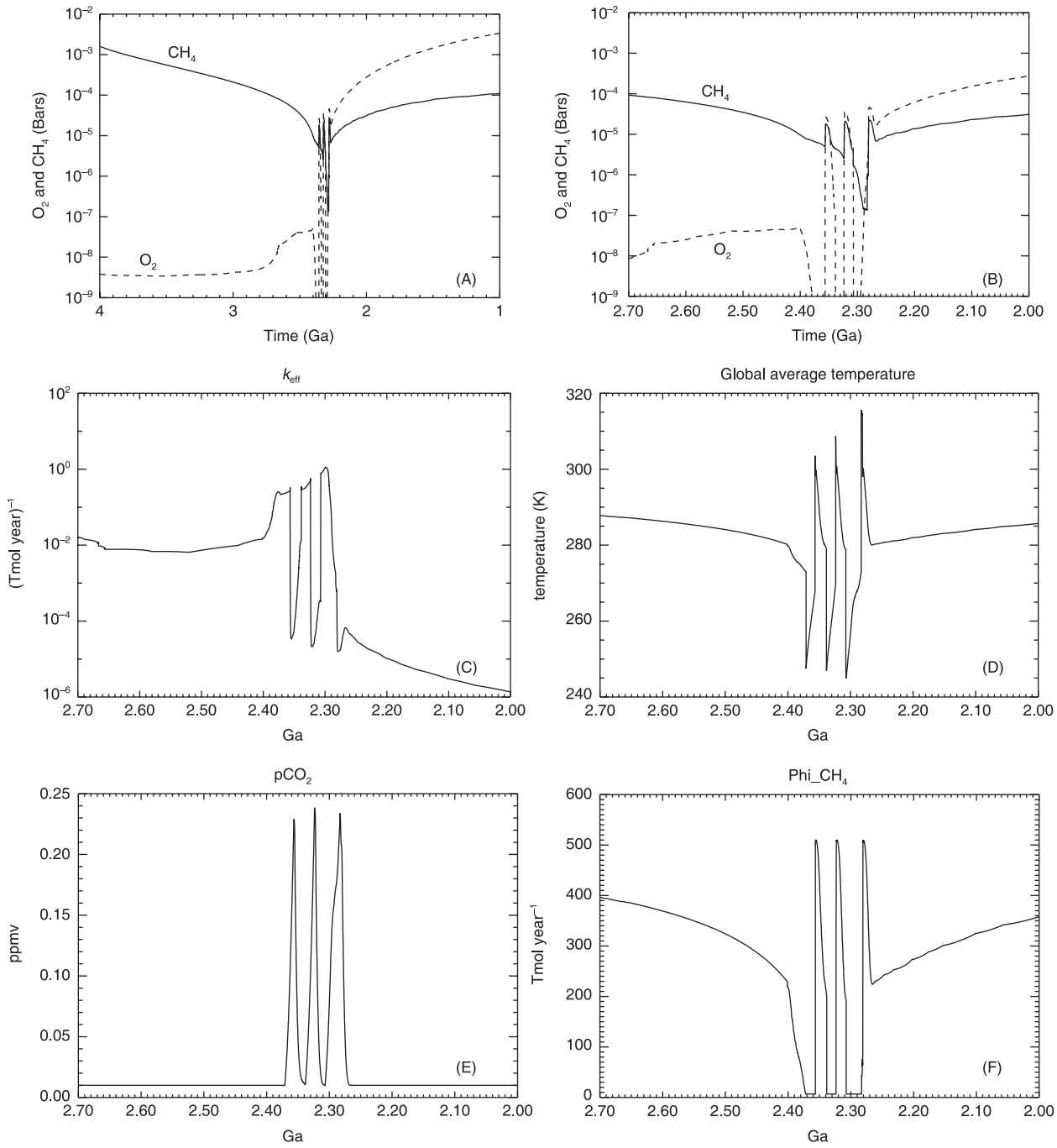

Fig. 13 Effect on the reference model from introducing the enhancements described in Section 7: Case 1 Temperature-dependent biosphere. Note the change in timescales between Fig. 13(A, B)–(F). (A) Atmospheric gases (bars) vs. time. (B) Same as 13A, zoomed in on transitional time period. (C) Atmospheric rate constant, k_{eff} vs. time. (D) Global average temperatures (K) vs. time. (E) Partial pressure of CO_2 (bars) vs. time. (F) Gross CH_4 flux into AOB, $\phi_{CH4,NEW}$ vs. time.

waters. To investigate the possibility that cyanobacterial productivity would be enhanced in a cooler climate, we use a parameterization similar to case 'A' of Lovelock & Kump (1994), shown as a dashed line on Fig. 12(B) and described in Table 1.

7.3 Model results with feedbacks

The effects of incorporating the above parameterizations into our reference model are shown in Figs 13 and 14, which illustrate our enhanced reference model with both our

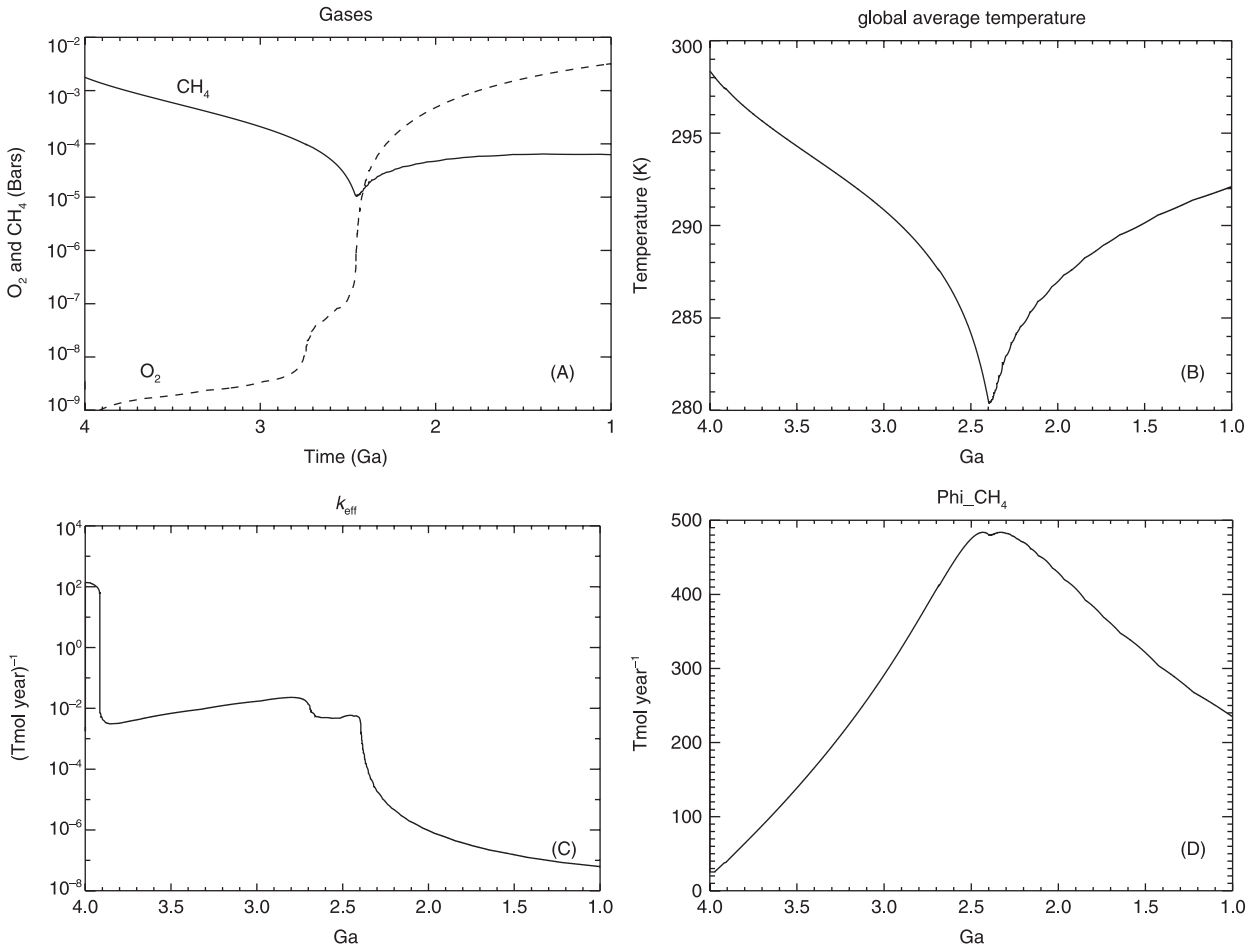

Fig. 14 Effect on the reference model from introducing the enhancements described in Section 7: Case 2 'Lovelock' temperature-dependent biosphere. (A) Atmospheric gases (bars) vs. time. (B) Global average temperatures (K) vs. time. (C) Atmospheric rate constant, k_{eff} vs. time. (D) Gross CH_4 flux into AOB, $\phi_{CH4,NEW}$ vs. time.

cyanobacterial growth curve (Case 1) and that of Lovelock & Kump (1994) (Case 2). The effect on the timing of the oxic transition is minimal in both cases (Figs 13A and 14A), lending strength to the general conclusions presented in Section 6. In both scenarios, global average temperatures reach their minimum value near the oxic transition (Figs 13D and 14B), and k_{eff} values (Figs 13C and 14C) are ~10^{-2} (Tmol year)$^{-1}$ prior to oxic transition, and decrease to ~10^{-6} (Tmol year)$^{-1}$ after. The primary difference is that Case 1 encounters 'Snowball Earth' conditions while Case 2 does not. The reason for this is primarily the effect of the temperature dependence of our coupled biosphere. Figure 13(F) reveals a global minimum of ϕ_{CH4} at the time of transition, while Fig. 14(D) shows a global maximum in ϕ_{CH4} at the time of transition. The solar luminosity is low enough at 2.4 Ga that the methane produced by the biosphere is vital in maintaining clement conditions. Once the CH_4 greenhouse collapses, CO_2 is the only remaining mobile greenhouse gas (other than the assumed presence of H_2O vapor, which has been accounted for in the temperature parameterizations). The 0.01 bar CO_2 level assumed here cannot maintain temperate conditions at 2.4 Ga without a significant flux of CH_4. The ice-albedo effect is turned on once global average temperatures fall below 3 °C in Case 1 (Fig. 13D), halting the sink on atmospheric CO_2. CO_2 rises to ~0.23 bar (Fig. 13E) before the greenhouse effect becomes strong enough to melt the ice. Once the ice melts, our simple carbon cycle attempts to re-establish CO_2 levels at 0.01 bar. This drops temperatures below 3 °C, re-establishing a 'Snowball Earth', although a fully temperature-dependent carbonate-silicate feedback (Walker *et al.*, 1981; Berner & Kothavala, 2001) might prevent such a re-occurrence. This oscillation in global temperatures repeats a third time, with CH_4 levels (Fig. 13B) dropping lower in each successive glaciation, until the biosphere regains control after the third event. The carbonate-silicate cycle and ice-albedo feedback represent complex systems that are difficult to model in a coupled AOB system without latitudinal extension, so we believe that the evolutionary details during our 'Snowball

Earth events' reflect the simplicity of the parameterizations rather than useful predictions of global biogeochemistry. We do note, however, that the temperature dependence of the biosphere can strongly affect the global average temperature, and that recovery from globally glaciated conditions is more likely with a thriving postmelting biosphere.

8. DISCUSSION

We have presented a quantitative model for the rise of oxygen based on a simplified atmospheric chemistry and evolving redox fluxes in the Earth system. Our numerical fluxes are computed self-consistently from reservoirs that evolve in redox-state to approximately modern values. We find that a geologically rapid oxic transition occurs when the sum of reductant fluxes from metamorphism and volcanic sources ($F_M + F_V$) drops below the flux of organic carbon burial F_B. These results provide numerical support to the hypothesis (Walker *et al.*, 1983; Kasting *et al.*, 1993; Catling *et al.*, 2001; Holland, 2002) that the geological fluxes of reducing volatiles and their rate of decrease set the timing of the oxic transition.

A perturbation analysis on the reference model shows that the amount of ferrous iron in the continental crust is the most sensitive parameter that affects the timing of the oxic transition. Increasing the modelled amount of iron in the continental crust increases the total mass of Fe^{2+} to be oxidized, which prolongs the amount of time that reducing gases emanate from the continental crust. In this way, the iron content of the crust can be thought of as a buffer that prevents the rise of oxygen even in the face of strong biological oxygen production from associated organic carbon burial. Once the buffer due to crustal iron content is overcome at the GOE, oxygen levels can rise to ~1% of present levels. After this point in time, other buffers likely become more important in regulating oxygen concentrations, with most attention focused on the biogeochemical cycles of sulfur and carbon (Canfield & Teske, 1996; Holland, 2002; Rothman *et al.*, 2003). Today, organic carbon burial is mostly balanced by oxidative weathering, where the oxidation of FeO is minor compared to oxidation of carbon and S^{2-}. Our model only contains a basic carbon cycle and does not include a sulfur cycle. Therefore, its predictive ability for the Proterozoic and Phanerozoic eons is limited. Future biogeochemical modelling that decouples the ocean from the atmosphere and considers carbon, sulfur, and iron cycling is needed to quantitatively explore the evolution of Earth's redox state during the second half of its history.

Another generic result of our model is that the oxic transition is inherently nonlinear. At the low CH_4 concentrations predicted once oxygen levels begin to rise, the loss of CH_4 is quantitatively balanced by atmospheric oxidation so that the term $k_{eff}[O_2][CH_4] \approx$ constant. However, k_{eff} depends on the atmospheric reservoir of oxygen $[O_2]$, and decreases with a thicker ozone layer. This causes O_2 to rise relatively sharply because O_2 losses decrease as O_2 increases, producing a positive feedback. Consequently, the GOE should occur relatively quickly in geological time. Recent geochemical evidence is consistent with this idea, as the South African craton reveals the disappearance of mass-independent sulfur isotope fractionation within ~100 Myr between 2.45 and 2.33 Ga (Bekker *et al.*, 2004). At the same time, tropospheric CH_4 levels are re-established to ~100 ppmv in our model in the Mesoproterozoic because the ozone layer shields tropospheric CH_4 from destruction. Thus, hydrogen escape to space continues as a persistent flux in the Proterozoic and could conceivably be implicated in a second rise of O_2, assuming a further buffer in the Earth system is overcome, perhaps associated with sulfur.

Hydrogen loss to space is a fundamental characteristic of terrestrial planets (Kasting & Catling, 2003), so all Earth-mass planets should become more oxidized with time as a consequence of this physical effect. Indeed, hydrogen loss is the widely accepted explanation for the surface oxidation states of Venus and Mars (Hunten, 1993). The surface materials of an abiotic planet with only F_V, F_M, and F_E acting will certainly oxidize as a result of these physical processes. But the presence of oxygenic photosynthesis and methanogenesis on Earth combined to significantly decrease the time to the oxic transition by (i) enhancing hydrogen escape via high levels of CH_4, and (ii) adding free oxygen into the Earth system. Indeed, for terrestrial planets in the habitable zone of their stars, substantial free O_2 build-up appears to require a biogenic source such as oxygenic photosynthesis (Kasting, 1997; Catling *et al.*, 2005). We have found that the fundamental timing of the transition from reducing to oxidizing conditions on a microbially inhabited Earth depends on the reductant inventory in the solid planet.

A final, more speculative, interpretation of our results relates to the proposed NASA and ESA missions (currently named Terrestrial Planet Finder (TPF) and DARWIN, respectively), which seek to infer the presence of oxygen in the spectra of atmospheres of extrasolar planets (Des Marais *et al.*, 2002). The proposed architecture requires weeks of integration time to obtain spectra with sufficient signal to noise, effectively limiting mission planners to ~50 targets over the mission lifetime. Given that our model shows that a fully inhabited Earth would not have undergone its first oxygen transition until 0.6 Ga if it had been endowed with five times more iron, target selection should take into consideration those planets most likely to be oxygenated, which from this preliminary analysis would be those of Earth mass or smaller for a terrestrial-type reductant inventory. A larger planet would, assuming a similar differentiation history, have a larger buffer of reduced materials to overwhelm in order to oxidize. Simulations show that the amount of iron delivered to 'potentially habitable' terrestrial planets can vary by factors of 2 with Earth on the 'high' end of possible iron contents (Raymond *et al.*, 2006a, b), indicating that other microbially inhabited Earth-like planets may contain less iron, and hence oxidize more quickly than the Earth did. The iron content of terrestrial planets has also been

shown to vary as a function of both the density distribution of the protoplanetary disc (Raymond *et al.*, 2005b) and the radial position of any giant planets in the system (Raymond *et al.*, 2005a); so planetary context is also important. These simulations do not formally calculate core/mantle partitioning, which will be necessary to understand the final distribution of iron in a planetary mantle. It remains possible that the iron contents of terrestrial planet mantles will vary more strongly based on stochastic late-stage impacts that postdate core formation. Future simulations that combine the theories of accretionary planet formation and the geophysics of high temperature collisions and core formation are needed to understand the range of iron contents that might be present in the upper mantle and crust of terrestrial planets.

8.1 Future work

Our model is a useful tool, but is highly simplified because important aspects of the Earth system are yet to be included. Such additions include additional climatic and physical feedbacks on the biosphere (i.e. limiting early CH_4 via organic haze), the details of how temperature structure bears on photochemistry, inclusion of the sulfur cycle, and crustal growth. Separating the atmosphere from the ocean would allow for a more accurate biosphere, although it would force us to take shorter timesteps. Further separating the ocean into upper and lower levels would allow for investigation of multiple stages of oxidation as predicted during the Proterozoic (Canfield, 2005) and Archean (Huston & Logan, 2004). Despite these suggestions for an enhanced model, our basic overall result – an oxic transition accompanied by a decrease of methane – remains a robust prediction, given the overall character of the equations and unidirectional hydrogen escape.

9. CONCLUSIONS

We have presented theoretical constraints on, and a self-consistent numerical model for, the rise of atmospheric oxygen at 2.4 Ga. Important results from analytical and numerical computations include:

1) Decreasing geological fluxes of reducing gases are a plausible cause of the oxic transition.

2) Metamorphic degassing from a more reduced Archean crust could have released more reductants into the atmosphere than in the present day, particularly in the form of methane.

3) The amount of reduced iron in the continental crust is likely a strong factor in the evolution of redox state of the crust and crustal fluids.

4) Methanogenesis promotes enhanced methane levels that warm the early Earth and compensate for a lower solar luminosity. However, the methane inevitably means that there is a greater rate of hydrogen escape, which ultimately drives oxidation of the lithosphere, a lowering of oxygen sinks, the rise of O_2, and glacial cooling. The atmosphere should jump from a state in which oxygen is a trace gas (<1 ppmv) to 1% of present levels (~0.002 bar) in a geologically short time due to the decreasing photochemical destruction of O_2 as the ozone layer forms. The reaction of the biosphere as Earth cools due to decreasing methane levels strongly affects the transitional atmosphere.

5) Other microbially inhabited Earth-like terrestrial planets could oxidize much earlier or later in their respective histories, so the consideration of planetary oxygen history is important in the search for astronomical biosignatures.

ACKNOWLEDGEMENTS

MC would like to thank Roger Buick and Jim Kasting for many helpful discussions. Thoughtful reviews by Dick Holland, Jim Kasting, and an anonymous reviewer greatly improved the quality and presentation of the manuscript. MC is supported by a NASA GSRP Fellowship NGT2-52295 at NASA Ames Research Center, NSF IGERT award DGE-9870713 to the University of Washington's Astrobiology Program, and by a grant from the ARCS Foundation. DC and KZ are supported by NASA Exobiology Program grants NNG04GJ95G and NNG05GGQ25G awarded to the University of Washington. DC also acknowledges support from a European Union Marie Curie Chair award.

REFERENCES

Aharon P (2005) Redox stratification and anoxia of the early Precambrian oceans: implications for carbon isotope excursions and oxidation events. *Precambrian Research* **137**, 207–222.

Ahrens TJ (1993) Impact erosion of terrestrial planetary atmospheres. *Annual Review of Earth and Planetary Sciences* **21**, 525–555.

Anbar AD, Knoll AH (2002) Proterozoic ocean chemistry and evolution: a bioinorganic bridge? *Science* **297**, 1137–1142.

Anders E, Grevesse N (1989) Abundances of the elements – meteoritic and solar. *Geochimica et Cosmochimica Acta* **53**, 197–214.

Arthur MA, Dean WE, Neff ED, Hay BJ, King J, Jones G (1994) Varve-calibrated records of carbonate and organic carbon accumulation over the last 2000 years in the Black Sea. *Global Biogeochemical Cycles* **8**, 195–217.

Barley ME, Bekker A, Krapez B (2005) Late Archean to Early Paleoproterozoic global tectonics, environmental change and the rise of atmospheric oxygen. *Earth and Planetary Science Letters* **238**, 156–171.

Beaumont V, Robert F (1999) Nitrogen isotope ratios of kerogens in Precambrian cherts: a record of the evolution of atmosphere chemistry? *Precambrian Research* **96**, 63–82.

Bebout BM, Carpenter SP, Des Marais DJ, Discipulo M, Embaye T, Garcia-Pichel F, Hoehler TM, Hogan M, Jahnke LL, Keller RM, Miller SR, Prufert-Bebout LE, Raleigh C, Rothrock M, Turk K (2002) Long-term manipulations of intact microbial mat communities in a greenhouse collaboratory: simulating Earth's present and past field environments. *Astrobiology* **2**, 383–402.

Bekker A, Holland HD, Wang PL, Rumble D, Stein HJ, Hannah JL, Coetzee LL, Beukes NJ (2004) Dating the rise of atmospheric oxygen. *Nature* **427**, 117–120.

Berman-Frank I, Lundgren P, Falkowski P (2003) Nitrogen fixation

and photosynthetic oxygen evolution in cyanobacteria. *Research in Microbiology* **154**, 157–164.
Berner RA (2004) *The Phanerozoic Carbon Cycle*. Oxford University Press, New York, pp. 150.
Berner RA, Beerling DJ, Dudley R, Robinson JM, Wildman RA (2003) Phanerozoic atmospheric oxygen. *Annual Review of Earth and Planetary Sciences* **31**, 105–134.
Berner RA, Kothavala Z (2001) GEOCARB III: a revised model of atmospheric CO_2 over phanerozoic time. *American Journal of Science* **301**, 182–204.
Betts JN, Holland HD (1991) The oxygen-content of ocean bottom waters, the burial efficiency of organic-carbon, and the regulation of atmospheric oxygen. *Global and Planetary Change* **97**, 5–18.
Beukes NJ, Dorland H, Gutzmer J, Nedachi M, Ohmoto H (2002) Tropical laterites, life on land, and the history of atmospheric oxygen in the Paleoproterozoic. *Geology* **30**, 491–494.
Bezos A, Humler E (2005) The Fe^{3+}/Sigma Fe ratios of MORB glasses and their implications for mantle melting. *Geochimica et Cosmochimica Acta* **69**, 711–725.
Bjerrum CJ, Canfield DE (2004) New insights into the burial history of organic carbon on the early Earth. *Geochemistry Geophysics Geosystems* **5**, Art. no. Q08001 (online).
Brocks JJ, Buick R, Summons RE, Logan GA (2003) A reconstruction of Archean biological diversity based on molecular fossils from the 2.78 To 2.45 billion-year-old Mount Bruce Supergroup, Hamersley Basin, Western Australia. *Geochimica et Cosmochimica Acta* **67**, 4321–4335.
Brocks JJ, Logan GA, Buick R, Summons RE (1999) Archean molecular fossils and the early rise of eukaryotes. *Science* **285**, 1033–1036.
Brocks JJ, Love GD, Summons RE, Knoll AH, Logan GA, Bowden SA (2005) Biomarker evidence for green and purple sulphur bacteria in a stratified Palaeoproterozoic sea. *Nature* **437**, 866–870.
Caldeira K, Kasting JF (1992a) The life span of the biosphere revisited. *Nature* **360**, 721–723.
Caldeira K, Kasting JF (1992b) Susceptibility of the early Earth to irreversible glaciation caused by carbon dioxide clouds. *Nature* **359**, 226–228.
Canfield DE (1998) A new model for Proterozoic ocean chemistry. *Nature* **396**, 450–453.
Canfield DE (2005) The early history of atmospheric oxygen: homage to Robert A. Garrels. *Annual Review of Earth and Planetary Sciences* **33**, 1–36.
Canfield DE, Habicht KS, Thamdrup B (2000) The Archean sulfur cycle and the early history of atmospheric oxygen. *Science* **288**, 658–661.
Canfield DE, Teske A (1996) Late-Proterozoic rise in atmospheric oxygen concentration inferred from phylogenetic and sulfur isotope studies. *Nature* **382**, 127–132.
Canil D (1999) Vanadium partitioning between orthopyroxene, spinel and silicate melt and the redox states of mantle sources regions for primary magmas. *Geochimica et Cosmochimica Acta* **63**, 557–572.
Catling DC (2006) Comment on 'A Hydrogen-Rich Early Earth Atmosphere'. *Science* **311**, 38a.
Catling DC, Claire MW (2005) How Earth's atmosphere evolved to an oxic state: a status report. *Earth and Planetary Science Letters* **237**, 1–20.
Catling DC, Glein CR, Zahnle KJ, McKay CP (2005) Why O-2 is required by complex life on habitable planets and the concept of planetary 'oxygenation time'. *Astrobiology* **5**, 415–438.
Catling DC, Zahnle KJ, McKay CP (2001) Biogenic methane, hydrogen escape, and the irreversible oxidation of early Earth. *Science* **293**, 839–843.
Chaloner WG (1989) Fossil charcoal as an indicator of paleoatmospheric oxygen level. *Journal of the Geological Society* **146**, 171–174.
Christensen UR (1985) Thermal evolution models for the Earth. *Journal of Geophysical Research-Solid Earth and Planets* **90**, 2995–3007.
Connolly JAD (1990) Multivariable phase-diagrams – an algorithm based on generalized thermodynamics. *American Journal of Science* **290**, 666–718.
Connolly JAD, Cesare B (1993) C-O-H-S fluid composition and oxygen fugacity in graphitic metapelites. *Journal of Metamorphic Geology* **11**, 379–388.
Coplen TB (1994) Reporting of stable hydrogen, carbon, and oxygen isotopic abundances. *Pure and Applied Chemistry* **66**, 273–276.
D'Hondt S, Rutherford S, Spivack AJ (2002) Metabolic activity of subsurface life in deep-sea sediments. *Science* **295**, 2067–2070.
Delano JW (2001) Redox history of the Earth's interior: implications for the origin of life. *Origins of Life and Evolution of the Biosphere* **31**, 311–341.
Des Marais DJ (2000) Evolution – when did photosynthesis emerge on Earth? *Science* **289**, 1703–1705.
Des Marais DJ, Harwit MO, Jucks KW, Kasting JF, Lin DNC, Lunine JI, Schneider J, Seager S, Traub WA, Woolf NJ (2002) Remote sensing of planetary properties and biosignatures on extrasolar terrestrial planets. *Astrobiology* **2**, 153–181.
Des Marais DJ, Strauss H, Summons RE, Hayes JM (1992) Carbon isotope evidence for the stepwise oxidation of the Proterozoic environment. *Nature* **359**, 605–609.
Donohue CL, Essene EJ (2000) An oxygen barometer with the assemblage garnet-epidote. *Earth and Planetary Science Letters* **181**, 459–472.
DuRand MD, Olson RJ, Chisholm SW (2001) Phytoplankton population dynamics at the Bermuda Atlantic Time-series station in the Sargasso Sea. *Deep-Sea Research Part II-Topical Studies in Oceanography* **48**, 1983–2003.
Dutkiewicz A, Volk H, George SC, Ridley J, Buick R (2006) Biomarkers from Huronian oil-bearing fluid inclusions: an uncontaminated record of life before the Great Oxidation Event. *Geology* **34**, 437–440.
Farquhar J, Bao H, Thiemans M (2000) Atmospheric influence of Earth's earliest sulfur cycle. *Science* **289**, 756–758.
Farquhar J, Wing BA (2003) Multiple sulfur isotopes and the evolution of the atmosphere. *Earth and Planetary Science Letters* **213**, 1–13.
Field CB, Behrenfeld MJ, Randerson JT, Falkowski P (1998) Primary production of the biosphere: integrating terrestrial and oceanic components. *Science* **281**, 237–240.
Finlayson-Pitts J, Barbara J, Pitts JN (2000) *Chemistry of the Upper and Lower Atmosphere: Theory, Experiments, and Applications.* Academic Press, San Diego, CA, pp. 969.
Frost BR (1991) Introduction to oxygen fugacity and its petrologic importance. In: *Reviews in Mineralogy* (ed. Lindsley DH). Mineralogical Society of America, Washington, D.C., pp. 1–9.
Garrels RM, Mackenzie FT (1971) *Evolution of Sedimentary Rocks.* Norton, New York, pp. 397.
Godderis Y, Veizer J (2000) Tectonic control of chemical and isotopic composition of ancient oceans: the impact of continental growth. *American Journal of Science* **300**, 434–461.
Habicht KS, Gade M, Thamdrup B, Berg P, Canfield DE (2002) Calibration of sulfate levels in the Archean ocean. *Science* **298**, 2372–2374.
Harries J, Ruth S, Russell JM (1996) On the distribution of mesospheric molecular hydrogen inferred from HALOE measurements of H_2O and CH_4. *Geophysical Research Letters* **23**, 297–300.

Hayes JM (1994) Global methanotrophy at the Archean-Preoterozoic transition. In: *Early Life on Earth* (ed. Bengtson S). Columbia University Press, New York, pp. 220–236.
Hayes JM, Waldbauer JR (2006) The carbon cycle and associated redox processes through time. *Philosophical Transactions of the Royal Society of London. Series B-Biological Sciences* **361**, 931–950.
Hinrichs KU (2002) Microbial fixation of methane carbon at 2.7 Ga: was an anaerobic mechanism responsible? *Geology Geochemistry Geophysics*, Volume 3, Article no. 1042 (online).
Hoehler TM, Bebout BM, DesMarais DJ (2001) The role of microbial mats in the production of reduced gases on the early Earth. *Nature* **412**, 324–327.
Hoffman PF, Schrag DP (2002) The Snowball Earth hypothesis: testing the limits of global change. *Terra Nova* **14**, 129–155.
Holland HD (1978) *The Chemistry of the Atmosphere and Oceans.* Wiley, New York, pp. 351.
Holland HD (1984) *The Chemical Evolution of the Atmosphere and Oceans.* Princeton University Press, Princeton, pp. 582.
Holland HD (2002) Volcanic gases, black smokers, and the Great Oxidation Event. *Geochimica et Cosmochimica Acta* **66**, 3811–3826.
Holland HD (2003) Discussion of the article by A. C. Lasaga and H. Ohmoto on 'The oxygen geochemical cycle: dynamics and stability', *Geochimica et Cosmochimica Acta* 66, 361–381, 2002. *Geochimica et Cosmochimica Acta* **67**, 787–789.
Holland HD (2006) The oxygenation of the atmosphere and oceans. *Philosophical Transactions of the Royal Society of London. Series B-Biological Sciences* **361**, 903–915.
Holser WT, Schidlowski M, Mackenzie FT, Maynard JB (1988) Geochemical cycles of carbon and sulfur. In: *Chemical Cycles in the Evolution of the Earth* (eds Gregor CB, Garrels RM, Mackenzie FT, Maynard JB). Wiley, New York, pp. 105–173.
Hornafius JS, Quigley D, Luyendyk BP (1999) The world's most spectacular marine hydrocarbon seeps (Coal Oil Point, Santa Barbara Channel, California): quantification of emissions. *Journal of Geophysical Research-Oceans* **104**, 20 703–20 711.
Houghton JT, ed. (1994) *Climate Change, 1994: Radiative Forcing of Climate Change and an Evaluation of the IPCC Is92 Emission Scenarios.* Cambridge University Press, Cambridge.
Huizenga JM (2001) Thermodynamic modelling of C-O-H fluids. *Lithos* **55**, 101–114.
Hunten DM (1990) Kuiper-Prize Lecture – escape of atmospheres, ancient and modern. *Icarus* **85**, 1–20.
Hunten DM (1993) Atmospheric evolution on the terrestrial planets. *Science* **259**, 915–920.
Hunten DM, Donahue TM (1976) Hydrogen loss from the terrestrial planets. *Annual Review of Earth and Planetary Sciences* **4**, 265–292.
Huston DL, Logan GA (2004) Barite, BIFs and bugs: evidence for the evolution of the Earth's early hydrosphere. *Earth and Planetary Science Letters* **220**, 41–55.
Junge CE, Schidlowski M, Eichmann R, Pietrek H (1975) Model calculations for the terrestrial carbon cycle: carbon isotope geochemistry and evolution of photosynthetic oxygen. *Journal of Geophysical Research* **80**, 4542–4552.
Kargel JS, Lewis JS (1993) The composition and early evolution of Earth. *Icarus* **105**, 1–25.
Karhu JA, Holland HD (1996) Carbon isotopes and the rise of atmospheric oxygen. *Geology* **24**, 867–870.
Kasting JF (1979) Evolution of oxygen and ozone in the Earth's atmosphere. *PhD Thesis*, University of Michigan, pp. 259.
Kasting JF (1988) Runaway and moist greenhouse atmospheres and the evolution of Earth and Venus. *Icarus* **74**, 472–494.
Kasting JF (1992) Models relating to Proterozoic atmospheric and oceanic chemistry. In: *The Proterozoic Biosphere: A Multidisciplinary Study* (eds Schopf JW, Klein C). Cambridge University Press, Cambridge, pp. 1185–1187.
Kasting JF (1997) Habitable zones around low mass stars and the search for extraterrestrial life. *Origins of Life* **27**, 291–307.
Kasting JF (2005) Methane and climate during the Precambrian era. *Precambrian Research* **137**, 119–129.
Kasting JF, Ackerman TP (1986) Climatic consequences of very high CO_2 levels in the earth's early atmosphere. *Science* **234**, 1383–1385.
Kasting JF, Brown LL (1998) Setting the stage: the early atmosphere as a source of biogenic compounds. In: *The Molecular Origins of Life: Assembling the Pieces of the Puzzle* (ed. Brack A). Cambridge University Press, New York, pp. 35–56.
Kasting JF, Catling DC (2003) Evolution of a habitable planet. *Annual Review of Astronomy and Astrophysics* **41**, 429–463.
Kasting JF, Donahue TM (1980) The evolution of atmospheric ozone. *Journal of Geophysical Research* **85**, 3255–3263.
Kasting JF, Eggler DH, Raeburn SP (1993) Mantle redox evolution and the oxidation state of the Archean atmosphere. *Journal* of. *Geology* **101**, 245–257.
Kasting JF, Pavlov AA, Siefert JL (2001) A coupled ecosystem-climate model for predicting the methane concentration in the Archean atmosphere. *Origins of Life and Evolution of the Biosphere* **31**, 271–285.
Kasting JF, Pollack JB, Crisp D (1984) Effects of high CO_2 levels on surface temperature and atmospheric oxidation state of the early earth. *Journal of Atmospheric Chemistry* **1**, 403–428.
Kemp AIS, Hawkesworth CJ (2004) Granitic perspectives on the generation and secular evolution of the continental crust. In: *Treatise on Geochemistry – Vol. 3: the Crust* (ed. Rudnick RL). Elsevier, Amsterdam, pp. 349–410.
Kenrick P, Crane PR (1997) The origin and early evolution of plants on land. *Nature* **389**, 33–39.
Kharecha P, Kasting JF, Siefert J (2005) A coupled atmosphere-ecosystem model of the early Archean Earth. *Geobiology* **3**, 53–76.
Kirschvink JL (1992) Late Proterozoic low-latitude global glaciation: the Snowball Earth. In: *The Proterozoic Biosphere* (eds Klein JW, Sa C). Cambridge University Press, Cambridge, pp. 51–52.
Knoll AH, Carroll SB (1999) Early animal evolution: emerging views from comparative biology and geology. *Science* **284**, 2129–2137.
Kopp RE, Kirschvink JL, Hilburn IA, Nash CZ (2005) The paleoproterozoic snowball Earth: a climate disaster triggered by the evolution of oxygenic photosynthesis. *Proceedings of the National Academy of Sciences of the United States of America* **102**, 11 131–11 136.
Kral TA, Brink KM, Miller SL, McKay CP (1998) Hydrogen consumption by methanogens on the early Earth. *Origins of Life and Evolution of the Biosphere* **28**, 311–319.
Kulikov YN, Lammer H, Lichtenegger HIM, Penz T, Breuer D, Spohn T, Lundin R, Biernat HK (2006) A comparative study of the influence of the active young sun on the early atmospheres of Earth, Venus, and Mars. *Space Science Reviews*, in press.
Kump LR, Kasting JF, Barley ME (2001) The rise of atmospheric oxygen and the 'upside-down' Archean mantle. *Geology Geochemistry Geophysics* **2**, (online).
Kump LR, Seyfried WE (2005) Hydrothermal Fe fluxes during the Precambrian: effect of low oceanic sulfate concentrations and low hydrostatic pressure on the composition of black smokers. *Earth and Planetary Science Letters* **235**, 654–662.
Lecuyer C, Ricard Y (1999) Long-term fluxes and budget of ferric iron: implication for the redox states of the Earth's mantle and atmosphere. *Earth and Planetary Science Letters* **165**, 197–211.
Li ZXA, Lee CTA (2004) The constancy of upper mantle fO (2) through time inferred from V/Sc ratios in basalts. *Earth and Planetary Science Letters* **228**, 483–493.

Lindsay JF, Brasier MD (2002) Did global tectonics drive early biosphere evolution? Carbon isotope record from 2.6 To 1.9 Ga carbonates of Western Australian basins. *Precambrian Research* **114**, 1–34.

Lovelock JE, Kump LR (1994) Failure of climate regulation in a geophysiological model. *Nature* **369**, 732–734.

Manning CE, Ingebritsen SE (1999) Permeability of the continental crust: Implications of geothermal data and metamorphic systems. *Reviews of Geophysics* **37**, 127–150.

McDonough WF, Sun S-S (1995) Composition of the Earth. *Chemical Geology* **120**, 223–253.

Melezhik VA, Fallick AE, Medvedev PV, Makarikhin VV (1999) Extreme C-13 (carb) enrichment in ca, 2.0 Ga magnesite-stromatolite-dolomite – 'red beds' association in a global context: a case for the world-wide signal enhanced by a local environment. *Earth-Science Reviews* **48**, 71–120.

Melezhik VA, Fallick AE, Rychanchik DV, Kuznetsov AB (2005) Palaeoproterozoic evaporites in Fennoscandia: implications for seawater sulphate, the rise of atmospheric oxygen and local amplification of the delta C-13 excursion. *Terra Nova* **17**, 141–148.

Melnik YP (1982) *Precambrian Banded Iron-Formations: Physicochemical Conditions of Formation*. Elsevier, Amsterdam, pp. 310.

Milkov AV, Etiope G (2005) Global methane emission through mud volcanoes and its past and present impact on the Earth's climate-a comment. *International Journal of Earth Sciences* **94**, 490–492.

Milkov AV, Sassen R, Apanasovich TV, Dadashev FG (2003) Global gas flux from mud volcanoes: a significant source of fossil methane in the atmosphere and the ocean. *Geophysical Research Letters* **30**, (9) 1–4.

Moisan JR, Moisan TA, Abbott MR (2002) Modelling the effect of temperature on the maximum growth rates of phytoplankton populations. *Ecological Modelling* **153**, 197–215.

Moore LR, Goericke R, Chisholm SW (1995) Comparative physiology of *Synechococcus* and *Prochlorococcus* – influence of light and temperature on growth, pigments, fluorescence and absorptive properties. *Marine Ecology-Progress Series* **116**, 259–275.

Morner NA, Etiope G (2002) Carbon degassing from the lithosphere. *Global and Planetary Change* **33**, 185–203.

Nakamura K, Kato Y (2004) Carbonatization of oceanic crust by the seafloor hydrothermal activity and its significance as a CO_2 sink in the Early Archean. *Geochimica et Cosmochimica Acta* **68**, 4595–4618.

Ohmoto H (1996) Evidence in pre-2.2 Ga paleosols for the early evolution of atmospheric oxygen and terrestrial biota. *Geology* **24**, 1135–1138.

Ohmoto H, Kerrick D (1977) Devolatilization equilibria in graphitic systems. *American Journal of Science* **277**, 1013–1044.

Ono S, Eigenbrode JL, Pavlov AA, Kharecha P, Rumble D III, Kasting JF, Freeman KH (2003) New insights into Archean sulfur cycle from mass-independent sulfur isotope records from the Hamersley Basin, Australia. *Earth and Planetary Science Letters* **213**, 15–30.

Onstott TC, McGown D, Kessler J, Sherwood Lollar B, Lehmann KK, Clifford SM (2006) Martian CH_4: sources, flux, and detection. *Astrobiology* **6**, 377–395.

Partzsch GM, Lattard D, McCammon C (2004) Mossbauer spectroscopic determination of Fe^{3+}/Fe^{2+} in synthetic basaltic glass: a test of empirical fO (2) equations under superliquidus and subliquidus conditions. *Contributions to Mineralogy and Petrology* **147**, 565–580.

Patchett PJ, Arndt NT (1986) Nd isotopes and tectonics of 1.9–1.7 Ga crustal genesis. *Earth and Planetary Science Letters* **78**, 329–338.

de Pater I, Lissauer JJ (2001) *Planetary Sciences*. Cambridge University Press, New York, pp. 528.

Pavlov AA, Hurtgen MT, Kasting JF, Arthur MA (2003) Methane-rich Proterozoic atmosphere? *Geology* **31**, 87–90.

Pavlov AA, Kasting JF (2002) Mass-independent fractionation of sulfur isotopes in Archean sediments: strong evidence for an anoxic Archean atmosphere. *Astrobiology* **2**, 27–41.

Pavlov AA, Kasting JF, Brown LL (2001) UV-shielding of NH_3 and O_2 by organic hazes in the Archean atmosphere. *Journal of Geophysical Research* **106**, 23 267–23 287.

Pavlov AA, Kasting JF, Brown LL, Rages KA, Freedman R (2000) Greenhouse warming by CH_4 in the atmosphere of early Earth. *Journal of Geophysical Research* **105**, 11 981–11 990.

Pearson DG, Canil D, Shirey SS (2004) Mantle samples included in volcanic rocks: xenoliths and diamonds. In: *Treatise on Geochemistry – Vol. 2: the Mantle and Core* (ed. Carlson RW). Elsevier, Amsterdam, pp. 171–275.

Petsch ST (2004) The global oxygen cycle. In: *Treatise on Geochemistry – Vol. 8: Biogeochemistry* (ed. Schlesinger WH). Elsevier, Amsterdam, pp. 515–555.

Poulton SW, Fralick PW, Canfield DE (2004) The transition to a sulphidic ocean similar to 1.84 billion years ago. *Nature* **431**, 173–177.

Raghoebarsing AA, Pol A, van de Pas-Schoonen KT, Smolders AJP, Ettwig KF, Rijpstra WIC, Schouten S, Damste JSS, Op den Camp HJM, Jetten MSM, Strous M (2006) A microbial consortium couples anaerobic methane oxidation to denitrification. *Nature* **440**, 918–921.

Rasmussen B, Buick R (1999) Redox state of the Archean atmosphere: evidence from detrital heavy minerals in ca. 3250–2750 Ma sandstones from the Pilbara Craton, Australia. *Geology* **27**, 115–118.

Raymond SN, Quinn T, Lunine JI (2005a) The formation and habitability of terrestrial planets in the presence of close-in giant planets. *Icarus* **177**, 256–263.

Raymond SN, Quinn T, Lunine JI (2005b) Terrestrial planet formation in disks with varying surface density profiles. *Astrophysical Journal* **632**, 670–676.

Raymond SN, Quinn T, Lunine JI (2006a) High-resolution simulations of the final assembly of Earth-like planets 2: water delivery and planetary habitability. *Astrobiology*, in press.

Raymond SN, Quinn T, Lunine JI (2006b) High-resolution simulations of the final assembly of Earth-like planets I: terrestrial accretion and dynamics. *Icarus* **183**, 265–282.

Reeburgh WS, Ward BB, Whalen SC, Sandbeck KA, Kilpatrick KA, Kerkhof LJ (1991) Black-Sea methane geochemistry. *Deep-Sea Research Part a-Oceanographic Research Papers* **38**, S1189–S1210.

Rogers JJW, Santosh M (2004) *Continents and Supercontinents*. Oxford University Press, New York, pp. 289.

Ronov AB (1983) The earth's sedimentary shell: quantitative patterns of its structure, composition, and evolution. *AGI Reprint Series* – originally published *in International Geology Review V. 24, 1982*, **5**, 1–80.

Rothman DH, Hayes JM, Summons RE (2003) Dynamics of the Neoproterozoic carbon cycle. *Proceedings of the National Academy of Sciences of the United States of America* **100**, 8124–8129.

Rudnick RL, Gao S (2004) The composition of the continental crust. In: *Treatise on Geochemistry – Vol. 3: the Crustacean* (ed. Rudnick RL). Oxford University Press, pp. 1–64.

Rudnick RL, McDonough WF, O'Connell RJ (1998) Thermal structure, thickness and composition of continental lithosphere. *Chemical Geology* **145**, 395–411.

Runnegar B (1991) Precambrian oxygen levels estimated from the biochemistry and physiology of early eukaryotes. *Global and Planetary Change* **97**, 97–111.

Ruttenberg KC (2004) The global phosphorus cycle. In: *Treatise on Geochemistry – Vol. 8: Biogeochemistry* (ed. Schlesinger WH). Elsevier, Amsterdam, pp. 585–643.
Rye R, Holland HD (1998) Paleosols and the evolution of atmospheric oxygen: a critical review. *American Journal of Science* **298**, 621–672.
Sack RO, Carmichael ISE, Rivers M, Ghiorso MS (1980) Ferric-ferrous equilibria in natural silicate liquids at 1 bar. *Contributions to Mineralogy and Petrology* **75**, 369–376.
Schidlowski M (1988) A 3800-million-year isotopic record of life from carbon in sedimentary rocks. *Nature* **333**, 313–318.
Schidlowski M (2001) Carbon isotopes as biogeochemical recorders of life over 3.8 Ga of Earth history: evolution of a concept. *Precambrian Research* **106**, 117–134.
Silver LT, Chappell BW (1988) The Penisular Ranges Batholiths: an insight into the evolution of the Cordilleran batholiths of southwestern North America. *Transactions of the Royal Society of Edinburgh: Earth Science* **79**, 105–121.
Sleep NH (2005a) Dioxygen over geologic time. In: *Metal Ions in Biology Systems, Vol. 43 – Biogeochemical Cycles of Elements* (eds Sigel A, Sigel H, Sigel R). Taylor & Francis, Boca Raton, FL, pp. 49–73.
Sleep NH (2005b) Evolution of the continental lithosphere. *Annual Review of Earth and Planetary Sciences* **33**, 369–393.
Sleep NH, Bird DK (2007) Niches of the pre-photosynthetic biosphere and geologic preservation of Earth's earliest ecology. *Geobiology*, in press.
Sleep NH, Hessler AM (2006) Weathering of quartz as an Archean climatic indicator. *Earth and Planetary Science Letters* **241**, 594–602.
Sleep NH, Windley BF (1982) Archean plate tectonics – constraints and inferences. *Journal of Geology* **90**, 363–379.
Sleep NH, Zahnle KJ (2001) Carbon dioxide cycling and implications for climate on ancient Earth. *Journal of Geophysical Research* **106**, 1373–1399.
Summons RE, Bradley AS, Jahnke LL, Waldbauer JR (2006) Steroids, triterpenoids and molecular oxygen. *Philosophical Transactions of the Royal Society of London. Series B-Biological Sciences* **361**, 951–968.
Summons RE, Brocks JJ (2004) Sedimentary hydrocarbons, biomarkers for early life. In: *Treatise on Geochemistry – Vol. 8: Biogeochemistry* (ed. Schlesinger WH). Elsevier, Amsterdam, pp. 63–115.
Tang EPY, Tremblay R, Vincent WF (1997) Cyanobacterial dominance of polar freshwater ecosystems: are high-latitude mat-formers adapted to low temperature? *Journal of Phycology* **33**, 171–181.
Taylor SR, McLennan SM (1995) The geochemical evolution of continental crust. *Reviews in Geophysics* **33**, 241–265.
Teske A, Dhillon A, Sogin ML (2003) Genomic markers of ancient anaerobic microbial pathways: sulfate reduction, methanogenesis, and methane oxidation. *Biology Bulletin* **204**, 186–191.
Tian F, Toon OB, Pavlov AA, De Sterck H (2005) A hydrogen-rich early Earth atmosphere. *Science* **308**, 1014–1017.
Tyrell T (1999) The relative influences of nitrogen and phosphorus on oceanic primary production. *Nature* **400**, 525–531.
Valentine DL (2002) Biogeochemistry and microbial ecology of methane oxidation in anoxic environments: a review. *Antonie Van Leeuwenhoek International Journal of General and Molecular Microbiology* **81**, 271–282.
Walker JCG (1977) *Evolution of the Atmosphere*. Macmillan, New York, pp. 318.
Walker JCG (1990a) *Numerical Adventures with Geochemical Cycles*. Oxford University Press, pp. 210.
Walker JCG (1990b) Origin of an inhabited planet. In: *Origin of the Earth* (eds Newsom HE, Jones JH). Oxford University Press, New York, pp. 371–375.
Walker JCG, Brimblecombe P (1985) Iron and sulfur in the pre-biologic ocean. *Precambrian Research* **28**, 205–222.
Walker JCG, Hays PB, Kasting JF (1981) A negative feedback mechanism for the long-term stabilization of Earth's surface temperature. *Journal of Geophysical Research* **86**, 9776–9782.
Walker JCG, Klein C, Schidlowski M, Schopf JW, Stevenson DJ, Walter MR (1983) Environmental evolution of the Archean-Early Proterozoic Earth. In: *Earth's Earliest Biosphere: Its Origin and Evolution* (ed. Schopf JW). Princeton University Press, Princeton, NJ, pp. 260–290.
Walter FM, Barry DC (1991) Pre- and main-sequence evolution of solar activity. In: *The Sun in Time* (eds Sonett CP, Giampapa MS, Matthews MS). University of Arizona Press, Tucson, AZ, pp. 633–657.
Warren SG, Brandt RE, Grenfell TC, McKay CP (2002) Snowball Earth: ice thickness on the tropical ocean. *Journal of Geophysical Research-Oceans* **107**, 1–18.
Watson AJ, Donahue TM, Walker JCG (1981) The dynamics of a rapidly escaping atmosphere: applications to the evolution of Earth and Venus. *Icarus* **48**, 150–166.
Watson A, Lovelock JE, Margulis L (1978) Methanogenesis, fires and the regulation of atmospheric oxygen. *Biosystems* **10**, 293–298.
Watson RT, Rodhe H, Oeschger H, Siegenthaler U (1990) Greenhouse gases and aerosols. In: *Climate Change: the IPCC Scientific Assessment* (eds Houghton JT, Jenkins GJ, Ephraums JJ). Cambridge University Press, Cambridge, pp. 1–40.
Wedepohl KH (1995) The composition of the continental-crust. *Geochimica et Cosmochimica Acta* **59**, 1217–1232.
Wildman RA, Hickey LJ, Dickinson MB, Berner RA, Robinson JM, Dietrich M, Essenhigh RH, Wildman CB (2004) Burning of forest materials under late Paleozoic high atmospheric oxygen levels. *Geology*, 457–460.
Yang WB, Holland HD (2003) The Hekpoort paleosol profile in Strata 1 at Gaborone, Botswana: soil formation during the great oxidation event. *American Journal of Science* **303**, 187–220.
Young GM, Long DGF, Fedo CM, Nesbitt HW (2001) Paleoproterozoic Huronian basin: product of a Wilson cycle punctuated by glaciations and a meteorite impact. *Sedimentary Geology* **141**, 233–254.
Zahnle KJ (1986) Photochemistry of methane and the formation of hydrocyanic acid (HCN) in the Earth's early atmosphere. *Journal of Geophysical Research* **91**, 2819–2834.
Zahnle KJ, Claire MW, Catling DC (2006) The loss of mass-independent fractionation in sulfur due to a Paleoproterozoic collapse of atmospheric methane. *Geobiology*, doi: 10.1111/j.1472-4669.2006.00085.x.